The variability of the rootzone storage capacity in Austria

An exploration of its controls

Bart Veenings

TU Delft

The variability of the rootzone storage capacity in Austria

An exploration of its controls

by

Bart Veenings

to obtain the degree of Master of Science

at the Delft University of Technology,

to be defended publicly on Wednesday September 9, 2020 at 10:00 AM.

Student number:	4227131	
Supervisor:	Dr. M. Hrachowitz	
Thesis committee:	Dr. M. Hrachowitz,	TU Delft, Chairman
	Dr. R. van Nooyen,	TU Delft
	Dr. R. Taormina,	TU Delft

An electronic version of this thesis is available at `http://repository.tudelft.nl/`.

Frontpage: Christinamari, 2009, *Austrian landscape*,
https://www.flickr.com/photos/64750418@N04/5893830693

TU Delft

Summary

The rootzone storage capacity (S_r) is a crucial part of the hydrological cycle. This storage provides water access for vegetation, in order to meet the atmospheric water demand through transpiration. The spatio-temporal variability of S_r is not well represented in current hydrological and climate models. The root zone storage capacity receives rapidly increasing interest from scientists. Recent studies developed a climate-based method to determine S_r. This method is based on the insight that ecosystems efficiently adapt their rootzone storage capacity to survive a drought with a certain return period. However, this method requires a vast amount of data. Long hydrological time-series with a rather fine temporal resolution are required. These time-series are not always available for many poorly gauged catchments. Therefore, it is important to explore what is exactly controlling this S_r, and if we can eventually predict it.

This study aims to describe the spatial and temporal variability of S_r with a combination of climate and land cover variables in Austria for the study period 1982 - 2008. To anticipate on expected snowfall, a snowfall module is included and calibrated with the use of a MODIS satellite snow cover product. The most important climate and land cover variables are identified, using multiple linear regression analysis. The best performing regression models are selected with a diverse combination of variables. This is done by comparing 21 catchments across the central and eastern part of Austria. Additionally, a stationary time-series split method is used to explore how S_r is changing in time. Subsequently, another multiple linear regression analysis is performed to explore the controls of the dynamics of S_r for these catchments.

According to this study, the Run-off coefficient describes S_r best in all studied regression models. A multiple linear regression model compiled out of the Run-off coefficient and the seasonality index performed best with an R^2_{adj} of 0.8. The seasonality index seems to be specific for this study since the highest fraction of precipitation and evaporation coincides in summer.

Land cover seems of less importance for the estimation of S_r. However, no conclusion could be drawn for the importance of land cover types in the regression analysis considering the disputable applicability of the land cover data. Furthermore, the relations of fractional cropland cover and fractional forest cover with S_r are in contradiction with current literature.

Apart from the spatial relationships, it is discovered that on average S_r increased from the year 1992 onwards. However, no indisputable explanation is encountered (R^2_{adj} 0.55). The decreasing Run-off coefficient explains most of the increase in S_r. No conclusions could be drawn on the influence of land cover change on S_r, caused by a irregular land cover time-series.

Since the catchments in this study are rather humid and have similar seasonal patterns, it would be interesting to investigate if the discovered relationships are also valid for more arid and seasonal varying catchments. Also, it would be useful to investigate the unexpected relationship between land cover and S_r further.

Preface

This master thesis is the end-product of the master program Water Management at the faculty Civil engineering and Geosciences and thus my study period at Delft University of Technology. Starting my bachelor in Mechanical Engineering, I am happy that my study career led me, via my exchange period at DTU to the interesting field of hydrology.

I think that this explorative research gives more insight into the controls of the rootzone storage of vegetation. Fulfilling this research was a tough, challenging but above all interesting period. Wherein I have learned a lot in the field of hydrology and developed myself on a personal level. I am looking forward to apply this acquired knowledge in a future job.

I would like to thank my committee members: Markus, Ronald and Riccardo for their guidance and stimulating insights, from which I learned the most during this period. Finishing this thesis was not possible without the support of my parents, friends and my always supporting girlfriend Lieke. Thank you all for your support.

Bart Veenings
Delft, September 2020

Contents

Nomenclature

Abbreviations

DEM	Digital elevation model	
LOOCV	Leave-one-out-cross-validation	
MODIS	Moderate Resolution Imaging Spectroradiometer	
NDSI	Normalized difference snow index	[-]
$NDVI$	Normalized Difference Vegetation Index	[-]
NIR	Reflectance in Near Infrared spectrum	[-]
PCA	Principle component analysis	
RED	Reflectance in red(visible) spectrum	[-]

Symbols

C_M	Snowmelt degree-day factor	$[LT^{-1}\,^{\circ}C^{-}1]$
E	Total actual evaporation	$[LT^{-1}]$
E_a	Actual evaporation	$[LT^{-1}]$
E_i	Interception evaporation	$[LT^{-1}]$
E_p	Potential evaporation	$[LT^{-1}]$
E_T	Transpiration	$[LT^{-1}]$
I_{max}	Maximum interception storage	$[L]$
P_{liq}	Liquid water input	$[LT^{-}1]$
M	Snowmelt	$[LT^{-1}]$
P	Total precipitation	$[LT^{-1}]$
P_e	Effective precipitation	$[LT^{-1}]$
P_e	Effective precipitation	$[LT^{-1}]$
Q	Total discharge	$[LT^{-1}]$
SD	Storage deficit	[L]
S_i	Interception reservoir storage	$[L]$
S_r	The rootzone storage capacity	[L]
S_{rz}	Rootzone reservoir storage	$[L]$
S_s	Snow reservoir storage	$[L]$
T	Return Period	[T]
T_a	Air temperature	[°C]
T_t	Threshold temperature	[°C]

List of Figures

List of Tables

1

Introduction

The rootzone storage (S_r) is an essential part of the hydrological cycle. It full-fills the water needs of vegetation. Via this vegetation, an extensive amount of water is stored in the unsaturated zone is available for evaporation. Periods of drought can be survived with water stored in this volume. Moreover, S_r is an important parameter in hydrological models and in climate models (Dirmeyer et al., 2006). Therefore, a globally distributed S_r could enhance these models. S_r could not be observed directly. Consequently, an estimation of this volume needs to be made. Unfortunately, the prediction of S_r is not sufficient for these applications yet.

The most common method to estimate the volume of S_r is to investigate soil and vegetation properties, like root length and root density, collected via fieldwork. This fieldwork is labour intensive and measurements are point specific and therefore, lacking spatial coverage. With fieldwork comes inaccuracy, and uncertainties are easily introduced. Also, in difficult accessible terrain, usually data is scarce due to practicalities. With these deficiencies in mind, a new method is proposed.

Considering this, a method of determining the storage volume of the rootzone based on climate data could enhance hydrological and climate models significantly (Gao et al., 2014). With this new approach more data is available and hence models could be provided with more distributed data. The rootzone storage is equivalent to water storage vegetation needs, to overcome a certain period of drought. The period of drought that vegetation is able to survive is a good indicator to estimate the water storage volume necessary. Considering that plants survived droughts and therefore exist at a certain location, the vegetation created the most favourable environment (de Boer-Euser et al., 2016). Also, vegetation will invest as much carbon in their rooting system as strictly necessary, because they compete for other resources e.g. light.

The idea that ecosystems can adapt their root system to climatic conditions is more accepted nowadays. This dynamical behaviour is observed by Nijzink et al. (2016b), his work compared the rootzone storage before logging, during recovery and after regrowth of the vegetation. Since evolution resulted in vegetation that is capable of adapting their rootzone to find an optimum between water accessibility and carbon investment in their roots, vegetation will not create redundant rootzone storage (Kleidon, 2004).

Considering that there are still an enormous amount of poorly gauged basins across the world, an alternative method could contribute significantly to research in these areas (Sivapalan et al., 2003). With an increasing amount of available remote sensing products, the possibilities to predict behaviour in these ungauged basins are increasing. Furthermore, the length of the available time-series is increasing, which creates new possibilities.

1.1. Background

Current development in estimating S_r established on a water balance is built upon the method of Gao et al. (2014). His method is using the mass curving technique, treating S_r as a reservoir and estimating its volume depending on water outflow, water input and dry period length. The climate-based method was verified by de Boer-Euser et al. (2016), where this research is comparing the estimated volumes of S_r based on climate data and S_r based on soil samples. The climate-based method outperformed the soil sample-based method, especially in the wetter climates. The climate-based method is built on the assumption that vegetation is adapting its rootzone storage in such a way it can overcome a certain drought. The plausibility of this assumption was again confirmed by the research of Nijzink et al. (2016b). This research showed similar results for the climate-based method and the values resulting from calibrated hydrological models. The research further showed that the rootzone storage capacity decreased significantly after a recovery period from deforestation. This observation makes the hypothesis Milly and Dunne (1994), that ecosystems can adapt their rootzone to their water demands plausible.

According to Wang-Erlandsson et al. (2016), simulations for estimating S_r perform better when S_r is calculated with diverse drought return periods for different types of vegetation. This can be an indication that disparate survival strategies are used by various vegetation. Primarily forest ecosystems can survive longer periods of drought than areas containing a majority of grass and bushes (Brunner et al., 2015). This disparate survival strategy results in varying rootzone storage capacities (Kolb et al., 1990).

It is shown feasible that the rootzone storage is dynamically adapting to climatic factors (Nijzink et al., 2016b). Since climate and vegetation are related (Schenk and Jackson, 2002), De Boer-Euser et al. (2019) investigated the relationship between variability of S_r and climatic or vegetational variables and showed that there is a strong relation between S_r and climate. This research concluded that vegetation characteristics can be linked directly to S_r. However, a less strong relationship between S_r and land cover type was found. The weaker relationship could be introduced by the selection of the return period. Also, soil properties could be of indirect influence because it is influencing which vegetation could grow. Additionally, the heterogeneity of vegetation could have influenced the results.

The study of De Boer-Euser et al. (2019) is merely conducted for boreal regions. Therefore, the impact of climatic factors in general on S_r is difficult to determine since a smaller range of these variables is present in these regions. The abundance of a broad range of vegetation leaves also room for further research. Moreover, this study showed that there is no strong correlation between land cover type and S_r. This is slightly in contrast to the theory that vegetation is adapting its rooting system following from different survival strategies. The fact that climate parameters are correlating with S_r could strongly depend on the chosen climate parameter. Another interesting finding is that it seems that the timing of snowmelt is an import control of the rootzone storage.

1.2. Research Scope

The main problem in current research is that there is no clear and complete view on the effect of different land cover types on the rootzone storage. An assessment of the effect of climate variables, vegetation variables and vegetation on the rootzone storage capacity has been made in literature (De Boer-Euser et al., 2019). Nevertheless, the research was conducted for a specific (boreal) region. Since it is important to have a representative view on the rootzone storage, more different regions across the world have to be considered.

Furthermore, the effect of (changing) climate on S_r is not fully understood yet. De Boer-Euser et al. (2019) looked at the different climatic and vegetational variables to identify if it is describing the magnitude of S_r. However, it is important to see if these findings can be reproduced in a different region. Nijzink et al. (2016b) already showed that deforestation has considerable influence on S_r, but it did not show the effect of land cover change on a larger scale and did not include a snowfall component in his research.

Most previous studies investigated a simple single relationship between the climate and land cover variables and S_r. However, in these complex ecosystems, it is not likely that S_r depends on a single variable only, a combined effect should represent a more complete view. Therefore, this thesis aims to explore the combined

effect of land cover types and climatic variability on the rootzone storage. The goal is to find a relationship between respectively land cover, climate and S_r. In order to describe the Spatio-temporal variability of S_r. This will be achieved by answering the following questions:

- What are the spatial differences in root-accessible water volumes across different Austrian catchments?
- Are there differences in the temporal evolution of the root-accessible water volumes?
- Which vegetational and hydro-climatic parameters influence the spatial and temporal differences?

It is suspected that the relationship between vegetation type and rootzone storage should be significant since different vegetation types could have different survival strategies. Since literature showed the dynamic character of the rootzone storage, it is expected to see a variation across different (hydrological) environments. Since different studies have shown a dynamically adapting rootzone storage in case of human-induced large-scale land cover change, it could be expected that for smaller changes a trend in S_r will be visible.

1.3. Study area

This study is focussing on catchments inside the borders of Austria. During wintertime, snowfall and snow cover is present in Austria. Therefore, it is required to include a snow storage component in the hydrological model. Further, S_r is not investigated in this region and data was easily accessible. The hydrological data for this research is retrieved from Gaál et al. (2012) that is based upon the work of Merz et al. (2006). In the dataset are included catchments from different (hydrological) regions in Austria, at various elevation levels. The catchments mean elevations differ from below 200 meter up to mean elevations of 2500 meter. The topography of the country results in diverse amounts of precipitation. In the western alpine region, an amount of 2500 mm/year, containing a significant fraction of snowfall. In the more arid eastern lowlands, the mean annual precipitation is 400 mm year (Merz and Blöschl, 2009). The initial dataset is containing: temperature, potential evaporation, precipitation and discharge for 69 catchments. The time-series are mostly continuous and do not have longer periods of missing data inside the time-series.

2

Methodology

This chapter elaborates the process of method selection. The flowchart visualized in Figure 2.1 describes the workflow of this study as further explained in this chapter. The hydrological data, digital elevation model and land cover data will be used to delineate the catchment and to determine its characteristics. The rootzone derivation model and the calibration of its snow module will be described. Lastly, the different predictor variables will be described and the regression model method used for analysing the predictor variables' relationship with S_r.

In this research, the Budyko curve is used for multiple purposes since it is an insightful and simple framework in hydrology. The Budyko curve is an empirical relationship between potential evaporation, actual evaporation and precipitation (Budyko et al., 1974). The ratio between the long-term averages of the actual evaporation E_a and the precipitation P is defined as the Aridity Index, see eq. 2.1. The ratio between the long-term averages of the potential evaporation E_p and the precipitation P is defined as the Evaporative Index, see eq. 2.2. In Figure 2.2 catchments are represented as points in the Budyko framework. Following the theory, all catchments should be located approximately along the Budyko curve (Budyko et al., 1974). A catchments' evaporation is limited by the energy limit in case that there is not enough energy to evaporate all available precipitation. The Aridity Index will be smaller than 1 in this case. An Aridity Index greater than 1 indicates the water-limited regime. In case of insufficient water supply for the evaporation demand, catchments are limited by the water limit.

$$AI = \frac{\overline{E_p}}{\overline{P}} \tag{2.1}$$

$$EI = \frac{\overline{E_a}}{\overline{P}} \tag{2.2}$$

A catchment should reach a steady-state is the fundamental assumption for the Budyko curve. This assumption is valid for long-term water balances since the incoming and outgoing fluxes cancel out while ecosystems strive to a state of equilibrium. Movement in Budyko space involves physical changes in the corresponding catchment. A vertical shift in Budyko space could indicate that the precipitation partitioning in run-off and evaporation is altered. This shift in the evaporative index can be created by changing forest biomass (Donohue et al., 2007, Velde et al., 2014). Because increasing biomass results in increasing transpiration. On the other hand, a horizontal shift in Budyko space indicates an altering Aridity Index. The Aridity Index is a product a catchment's climate, therefore a horizontal shift could argue a change in the climate. Hence, the Budyko framework could not only be used as an assessment tool of catchment characteristics, it is also suitable for the analysis of the alternation of these characteristics.

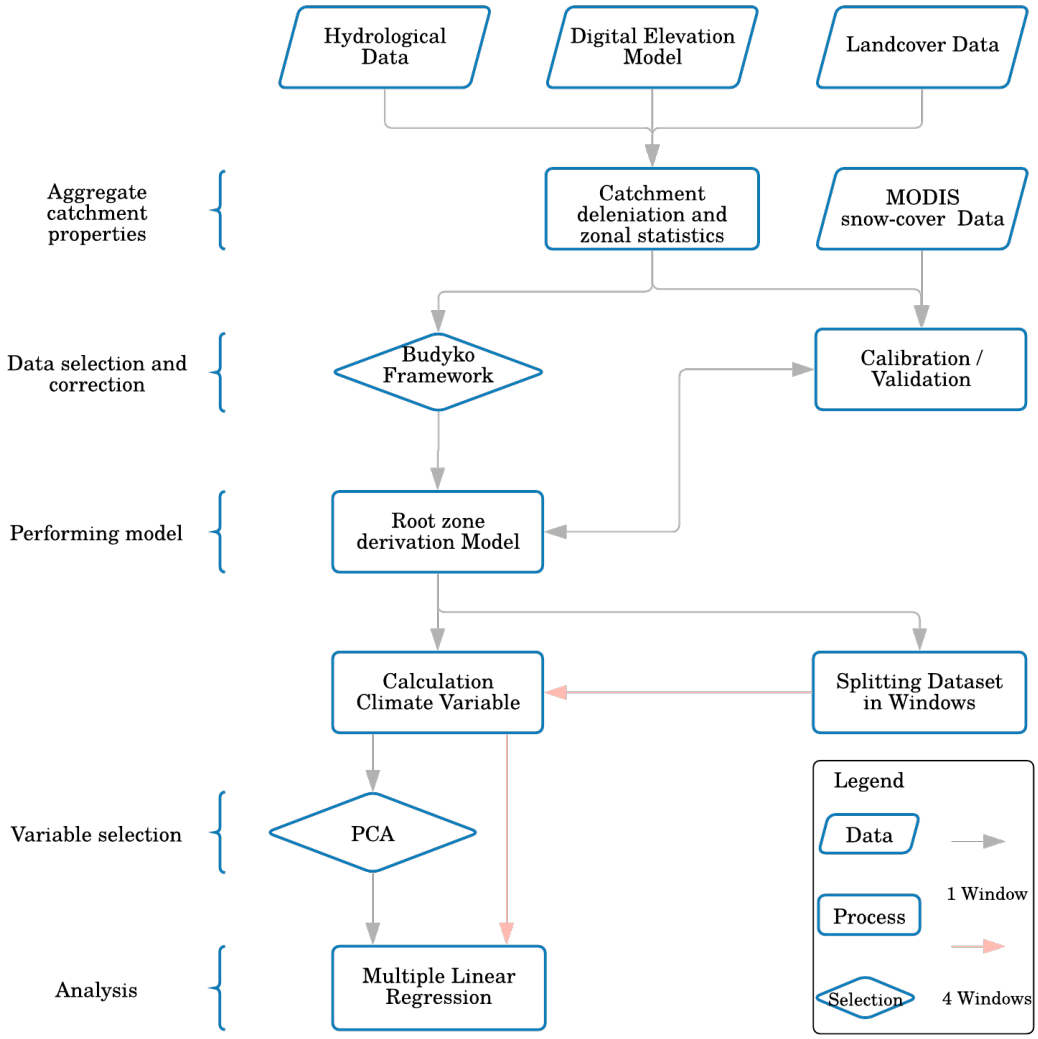

Figure 2.1: Flowchart presenting the action plan of this study.

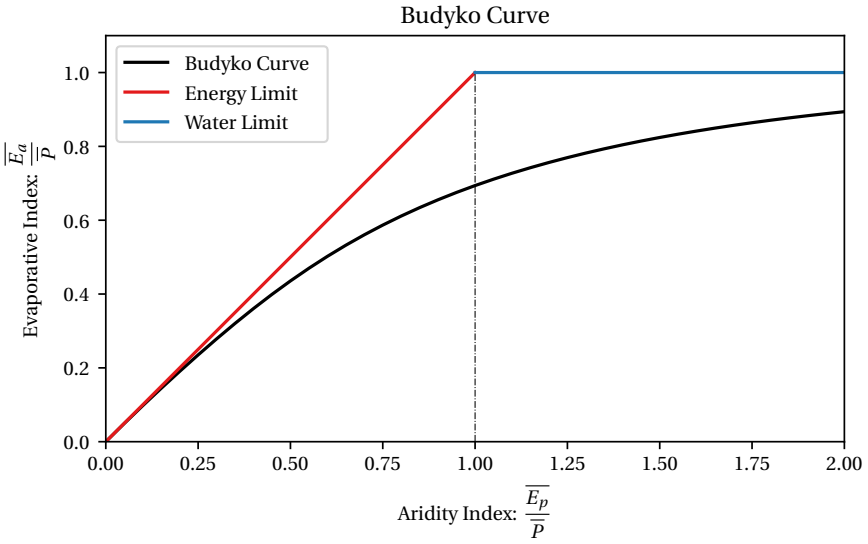

Figure 2.2: The Budyko-curve (Budyko et al., 1974) plotted on the Evaporative Index and Aridity Index. The Budyko space is constrained by the energy limit ($AI < 1$) and water limit ($AI > 1$).

2.1. Catchment selection

To ensure the quality and suitability of the data concerning this research, a screening was performed. The dataset is retrieved from Gaál et al. (2012), Merz et al. (2006) and precipitation and discharge are previously corrected by the authors. Precipitation is corrected because rain gauges are mainly located in the valleys. Moreover, the precipitation data is corrected because under-catch of snowfall occurs on higher elevations. Discharge data were screened and outliers were removed. Discharge stations with significant anthropogenic influence were excluded from the dataset. The climate graphs of the catchments are presented in Appendix B.

It is assumed that the potential evaporation from the dataset is based on temperature only. To verify this assumption, the temperature is calculated for the different elevation zones based on a temperature elevation relationship, see Section 2.3. With the use of the Thornthwaite equation and the relative size of the elevation zones, the catchments daily potential evaporation was calculated (Pereira and Pruitt, 2004). The result was corresponding with the dataset.

To check the integrity of the data, one could look at the outcome of a long-term water balance. The water balance showed in Equation 2.3, should theoretically close for longer periods. The storage change is assumed to be negligible over time compared to the other terms and therefore assumed to be zero. Accordingly precipitation P, should equal the sum of total evaporation E and discharge Q.

$$0 = \frac{dS}{dt} = P - E - Q \tag{2.3}$$

The evaporation data used in this study is the potential evaporation. Therefore, it is presumable that the water balance will not entirely add up to zero. Because the actual evaporation is mostly limited by water availability and will be therefore smaller than the measured potential evaporation. A positive water balance is assumed to result from defective data. A positive water balance might be valid, if the catchment delineation and the groundwater system are not overlapping (Bouaziz et al., 2018). Moreover, the existence of a glacier inside the catchment boundaries could cause a positive water balance due to glacier melt, especially in the west (Gaál et al., 2012). Since there is no data available for the groundwater flux and glacier melt, the positively balanced catchments are not included in this research.

Data of the different catchments are plotted in Budyko space, see Figure 2.5. From this figure one could observe outliers remotely located from the Budyko-curve. Also data points are visible above the energy limit. It is not physically possible to evaporate more water than possible with the energy available. The corresponding catchments are excluded from this research. A spatially overview of the selected catchments is displayed on the map of Figure 2.3. (European Union, Copernicus Land Monitoring Service 2020, 2020).

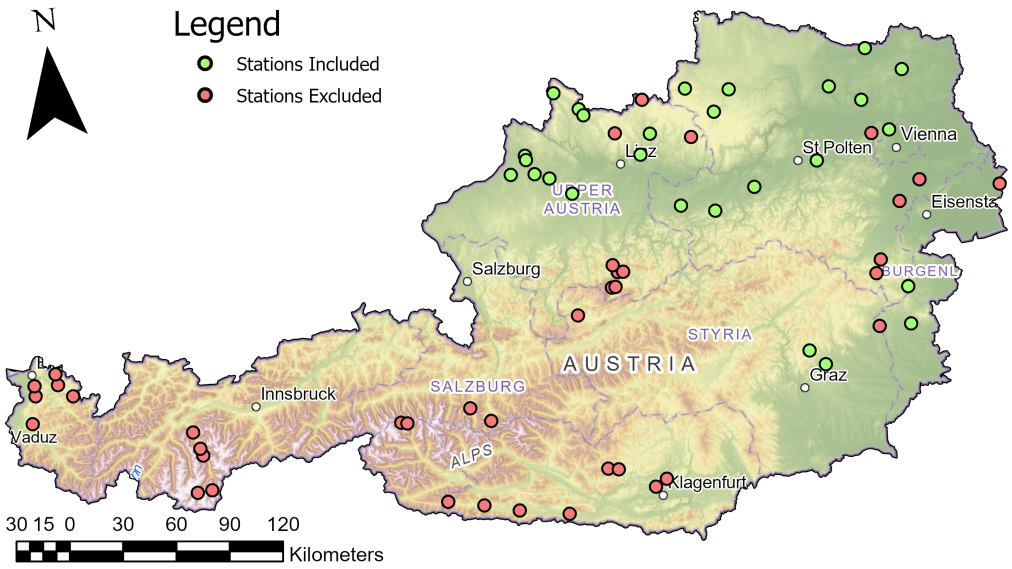

Figure 2.3: Overview of catchments selected for the analysis, the green-marked catchments are included in this study. The red-marked catchments are excluded due to ineligible data.

2.2. Watershed delineation

From the location of the discharge measurement stations, the corresponding catchment area and its boundaries are delineated. The catchments are delineated based on a digital elevation model. The delineation is conducted with the use of GRASS7, a tool for analysing geospatial data. The process will be shortly described and is schematized in Figure 2.4 for clarity. First, a flow direction model is created from the digital elevation map. Second, a flow accumulation model is created. After this the pour points are selected, those are the locations where discharge is measured. Therefore, the pour points are intersecting the locations of the discharge measuring stations. From these pour points the upstream catchment is determined. The digital elevation model used "EU-DEM v1.0", is a product of combined ASTER and SRTM data. The spatial resolution of the model is 25 meter.

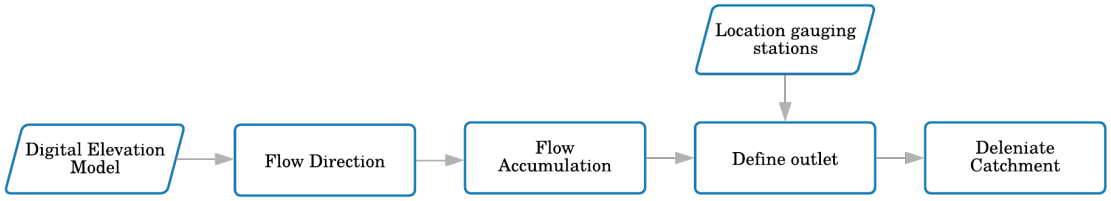

Figure 2.4: Flowchart presenting the catchment delineation process. The catchment is solely delineated based on a Digital Elevation Model and the location of the discharge gauging station.

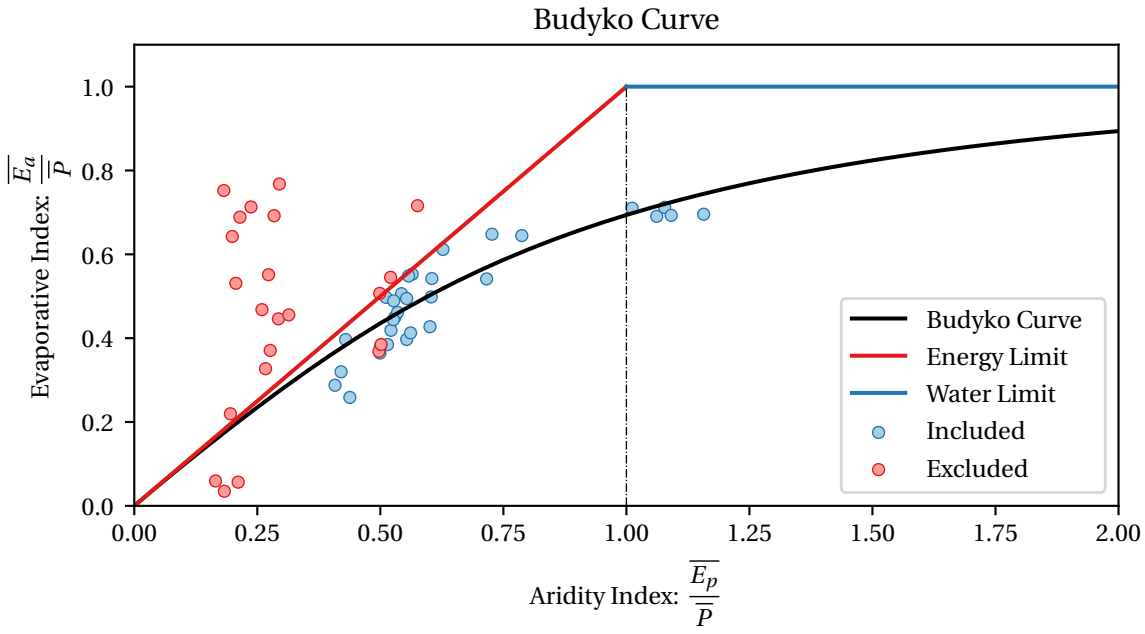

Figure 2.5: The Budyko framework is used to make a first selection which catchments are suitable for this research. The red catchments are excluded and the blue catchments are included. Part of the red catchment fall outside of the feasible spectrum due energy constraints. Other catchments are excluded while the water balance is not closing. The Evaporative and Aridity Index are based on long-term water balances.

2.3. Derivation of S_r

In this study, a simple bucket model is used to describe the fluxes and storages of the rootzone storage, snow storage and interception storage, the model structure is visualised in Figure 2.6. The bucket model is based on the models from Gao et al. (2014) and De Boer-Euser et al. (2019).

The model comprises an interception reservoir, snow reservoir and a rootzone reservoir. The interception reservoir has liquid precipitation as input, the outgoing fluxes of the reservoir are: interception evaporation E_i and effective precipitation P_e, these fluxes are described in eqs. (2.4) and (2.5). Effective precipitation is present given that the storage threshold (I_{max}) of the interception reservoir is reached. I_{max} represents the maximum amount of precipitation which can be stored at the canopy. For this study, a maximum interception storage threshold of 1.5 mm is assumed. A sensitivity analysis is performed to test the effect of different interception storage thresholds on S_r. And showed the low influence of I_{max} on the calculated S_r.

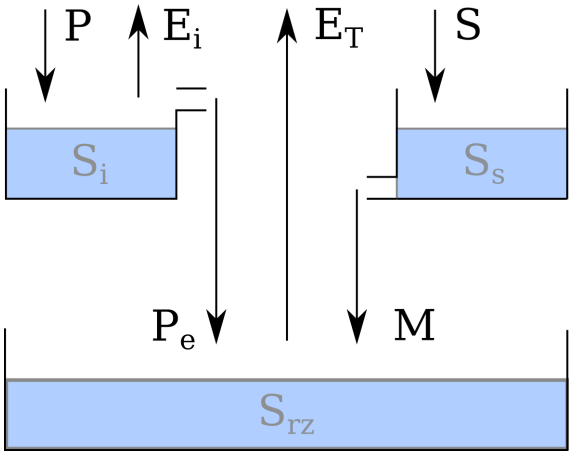

Figure 2.6: Schematisation of the bucket model used to calculate S_r. The incoming water flux is divided in precipitation and snowfall based on a threshold temperature. The model comprises an interception reservoir (S_i) with outflow effective precipitation. Snowfall is stored in a snow reservoir (S_s) until the melt threshold temperature is exceeded. The balance between effective precipitation, snowmelt and transpiration are resulting in a storage deficit in the rootzone reservoir (S_{rz}) which is used for the calculation of the rootzone storage capacity.

$$E_i = \begin{cases} E_p, & \text{if } E_p\,dt < S_i \\ \frac{S_i}{dt}, & \text{if } E_p\,dt \geq S_i \end{cases} \tag{2.4}$$

$$P_e = \begin{cases} 0, & \text{if } S_i \leq I_{\max} \\ \frac{S_i - I_{\max}}{dt}, & \text{if } S_i > I_{\max} \end{cases} \tag{2.5}$$

The snow reservoir has one input, snowfall. The total precipitation is divided into snowfall or liquid precipitation according to an atmospheric threshold temperature(T_{Tr}). This T_{Tr} is following from the calibration and validation process described in 2.4. The output of the snow reservoir is the snowmelt (M), which is depending on this same threshold temperature.

Lastly, the rootzone reservoir is modelled as an infinite reservoir. This theoretical infinite reservoir can contain an infinite amount of water. Effective precipitation and snowmelt are the incoming fluxes of the rootzone reservoir. The outgoing flux of the rootzone reservoir is the transpiration of vegetation. Since transpiration is not a measured quantity, it is estimated based on closing the long-term water balance. Equation 2.6 shows how the long-term average transpiration is calculated. Which can be applied since it is assumed that the transpiration is the only form of evaporation in the rootzone reservoir.

$$\overline{E_T} = \overline{P_e} + \overline{M} - \overline{Q} \tag{2.6}$$

Since we need daily transpiration, the total transpiration is divided over time proportional to the magnitude of the potential evaporation. Hence, the daily transpiration cannot exceed the potential evaporation. Equation 2.7 shows the daily transpiration $E_{T,d}$ as a result of scaling with the daily potential evaporation $E_{p,d}$ and the fraction of the long-term averages of the transpiration $\overline{E_T}$ and the potential evaporation $\overline{E_p}$.

$$E_{T,d} = E_{p,d} \times \frac{\overline{E_T}}{\overline{E_p}} \tag{2.7}$$

To determine the volume of the rootzone storage, it is required to calculate the storage deficit. The storage deficit increases when the transpiration demand is bigger than the liquid water supply. The cumulative storage deficit is estimated over time and is described in Equation 2.8. The maximal cumulative storage deficit is calculated for every hydrological year.

The start of the hydrological year is defined as the month after the wettest month of the year. Usually, the storage deficit is returned to zero at the wettest period at the start of the hydrological year or at least every 3 hydrological years. However, in some cases, a severe period of drought results in the fact that the storage deficit is not returned to zero after 3 years. In these cases, an iterative approach from van Oorschot (2020) is used to correct for this long-term deficit for this specific catchments. This approach is based on a non-closing yearly water balance. The method assumes that in case of overlong droughts, transpiration is overestimated since water availability limits this. The difference in storage deficit at the end of the year is used to calculate the transpiration which is necessary to return to a storage deficit of zero, see Equations: 2.10, 2.11 and 2.12. Where the a denotes yearly totals. This process is repeated until a converging result.

$$SD = \int_{t_0}^{t_1} (P_e - E_T)\, dt \tag{2.8}$$

Where t_0 and t_1 are the start time and end time of the time-series. Using Equation 2.8 the yearly storage deficits are calculated. This yearly storage deficit is visualized in Figure 2.7. The occurrence of these extreme droughts is used for estimating S_r.

To compare droughts with varying magnitudes across different catchments, a definition of its extremity is necessary. A proven tool for comparison of extreme droughts is to examine the return period of a drought. The return period is specified as the period in which an event is likely to occur. The return period can be determined by using an extreme value distribution. According to Gao et al. (2014) and Wang-Erlandsson et al. (2016), the storage deficit with a return period of 20 years is most suitable as an averaged catchment representative. However, the optimal catchment representative return period differs per catchment.

During this study, the 20-year return period is used for analysis, hence the catchment storage deficits are compared for the same return period. For the temporal analysis, a different return period is used, as discussed in 2.7. The most common extreme value distribution families are Gumbel, Fréchet and Weibull combined in the Generalized Extreme Value distribution (GEV). In this research, the Gumbel extreme value distribution type 1 is used (Gumbel, 1941).

The yearly storage deficits are fit to this distribution by adjusting its location and scale parameter. Based on this distribution, the storage deficit can be calculated associated with a 20-year return period. The reduced variate (y) is used to link the return period to the yearly maximum storage deficit. This maximum deficit is defined as the difference between the maximum and minimum storage deficit in a year.

$$y = -\ln\left(-\ln\left(1 - \frac{1}{T}\right)\right) \tag{2.9}$$

Where: T is the return period of yearly maximum storage deficit.

The Gumbel type 1 used in earlier studies, these studies showed that the rootzone storage capacity is performing better than other methods for the determination of S_r(de Boer-Euser et al., 2016, De Boer-Euser et al., 2019, Gao et al., 2014). To reduce differences in errors between this study and the current literature, the Gumbel type 1 distribution is used in this study. However, other extreme value distributions could describe the distribution of storage deficits better.

$$\frac{dS_a}{dt} = \frac{SD(t_0) - SD(t_1)}{t_0 - t_1} \tag{2.10}$$

$$\overline{E_{T,a}} = \overline{P_{e,a}} + \overline{M_a} - \overline{Q_a} - \frac{dS_a}{dt} \tag{2.11}$$

$$E_{T,d} = E_{p,d} \times \frac{\overline{E_{T,a}}}{\overline{E_{p,a}}} \tag{2.12}$$

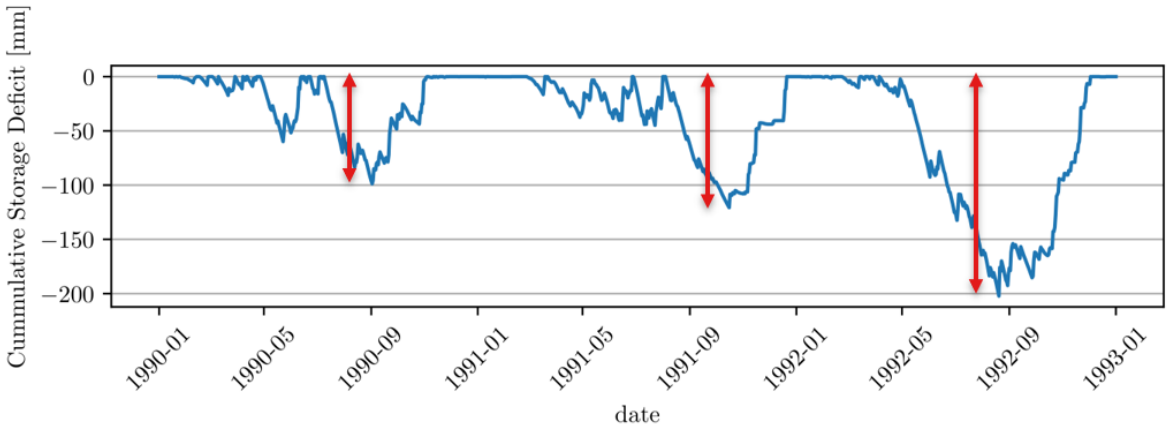

Figure 2.7: The cumulative storage deficit in millimetre from 1990-1992 in catchment 204859. The cumulative storage deficit is calculated with a daily resolution. The red arrows indicate the maximum storage deficit for each specific year. Those yearly maxima are used to determine S_r

Considering the significant elevation differences within a single catchment, a distinction between elevation levels is needed because the temperature at these different elevations forces diverse processes. While temperature is decreasing with increasing elevation, assumed was a decrease of 0.6 °C/100m, which is comparable with findings of Kirchner et al. (2013). For example, the temperature is the main driver of the modelled snowmelt and snowfall. Resulting in that different elevation zones will experience diverse amounts of snowmelt and snow cover. From this follows a different timing of meltwater available to vegetation. This timing could be important for the storage deficit estimations when this moment coincides with the onset of evaporation. Each elevation zone has a different surface area, therefore the contribution of the elevation to the water balance of the catchment is alternating. For every catchment, the snowmelt from the elevation zones is weighted with the zones corresponding surface area.

The fluxes and storages are numerically modelled in Python 3.6. Python is a high-level programming language with many developed open-source modules available. The code corresponding to the hydrological model is provided in Appendix A.

2.4. Snow cover calibration

Significant amounts of snow are expected to fall during the winter months. However, no snowfall data is included in the dataset used for this study. Therefore, another method to retrieve and subsequently model snowfall and melt is necessary. A temperature index method is used to model the amount of snowfall and melt. If snow is present in the snow reservoir, the snow melt (M) is modelled according to Equation 2.13 (Hock, 2003).

$$M = \begin{cases} M = C_M \times (T_a - T_t) & \text{if } T_a > T_t \\ 0, & \text{if } T_a < T_t \end{cases} \tag{2.13}$$

Where C_M denotes a constant for the amount of melt in millimetre per degree Celsius. T_a denotes the air temperature and T_t a threshold temperature from which the snow melts.

To deduce the snowfall from the total precipitation, T_t is used as for the snowmelt. This collective threshold temperature is used for sake of simplicity during the calibration process and minimizing computational demand. In reality, the threshold temperature will differ in the processes of snow accumulation and ablation. However, the temperatures will be close. The T_t and C_M are determined for every catchment via a calibration and validation process. The MODIS Terra(MOD10A1) daily snow cover product is used (Hall and Riggs, 2016) to observe snow cover. Daily snow cover is obtained from satellite imagery as a value for the Normalized Difference Snow Index (NDSI). This index is the relative magnitude of the reflectance difference among the

visible and short-wave infrared spectrum. It is assumed that for NDSI > 0.4 the corresponding pixel is covered with snow (Klein et al., 1998). Per elevation zone is estimated if the majority of this zone has snow cover. For every elevation zone, this results in a discrete time-series which represents snow cover at a given time.

The following step is to compare the MODIS time-series to the modelled snow cover. To achieve this, the snow dynamics were modelled for a set of combinations of C_M and T_t, the snowfall and snowmelt were calculated for each combination. This modelled snow cover is compared with the MODIS snow cover. For multiple combinations of C_M and T_t. For each day the difference between modelled snow cover days and snow cover days resulting from the MODIS product was calculated. Since a discrete approach is used, 1 for snow cover and 0 for no cover, the result for every time-series are summed and thereafter minimized using the combinations of C_M and T_t. The calibration period lasted from summer 2001 to summer 2006. During this period the MODIS data was mostly complete. Nevertheless, due to the obstruction of clouds, a significant amount of days were not included in the calibration. Starting the calibration in summer is necessary since the non-eternal snow should be melted. In Figure 2.8 an example catchment is displayed. Here one could see the different elevation zones and the snow cover classification for a random single day.

After the calibration is performed the 10 best-performing calibrations were validated on the period lasting from summer 2006 to summer 2008. From this validation, the combinations of C_M and T_t, resulting in the lowest non-matching days between the modelled and observed snow cover were selected for each catchment.

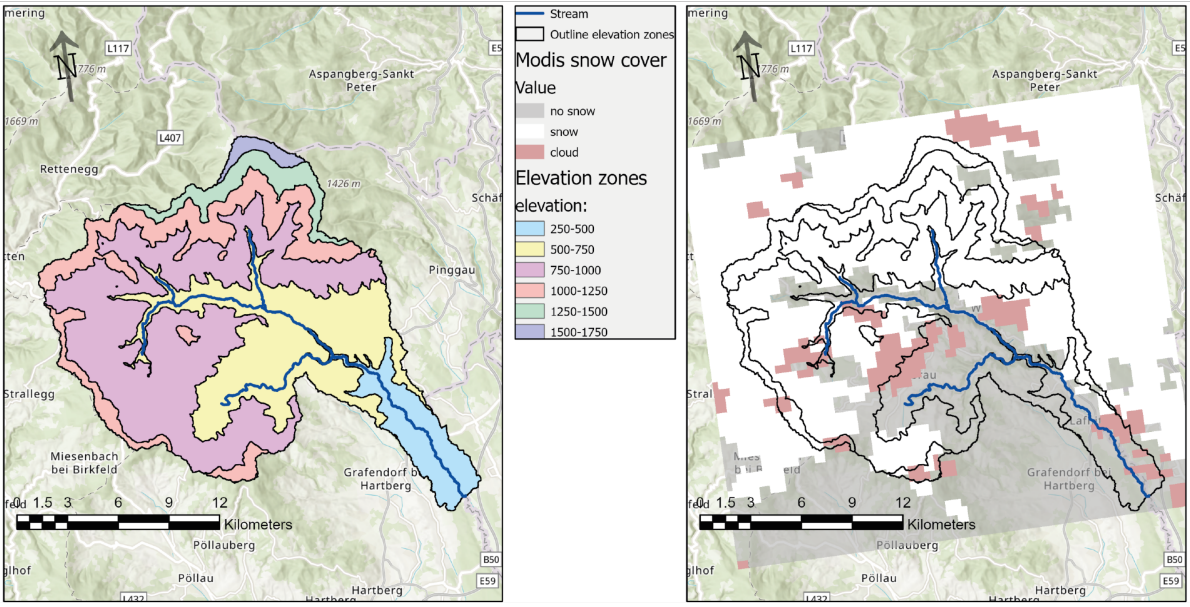

Figure 2.8: Graphical overview of Catchment 211680 (Not part of this study). **(a)** Illustrates the different elevation zones. **(b)** The snow cover classification for a random single day. Where for each elevation zone the majority of a classification is selected for the calibration.

2.5. Regression analysis

2.5.1. Regression method

A statistical analysis has to be performed to discover a relationship between the different catchment characteristics and the calculated rootzone storage. Since the amount of catchment considered in this study is rather small, the statistical methods applicable are reduced. Firstly, simple linear regression can be used to describe the relationship between each variable and S_r individually (De Boer-Euser et al., 2019). However, the correlations between different predictor variables and S_r can be ambiguous, since multiple variables influence S_r at the same time. Therefore, one could use multiple linear regression to find the combined effect of the different variables on S_r. Furthermore, regularization methods like, Lasso and Ridge regression are usable to detect relationships. However, those methods are less intuitive as multiple linear regression. More-

over, it seems that these regularization methods are less suitable for small datasets. Therefore, a multiple linear regression is applied.

To apply multiple linear regression one should take into account the following conditions:

- Relationship should be approximately linear
- Constant error variance
- Independent errors terms
- Normal errors
- No multi-collinearity
- Exogeneity

The relationships are most likely not strictly linear. Yet, for the sake of model simplicity, it is assumed that S_r can described as a linear combination of the variables, see equations, 2.14 and 2.15. It is strived to reduce collinearity, using data selection methods, see e.g. 2.5.2. After analysis, the behaviour of the error terms is evaluated.

$$\hat{Y} = \hat{\beta}_0 + \hat{\beta}_1 X_1 + \cdots + \hat{\beta}_p X_p \tag{2.14}$$

$$Y = \hat{Y} + \epsilon \tag{2.15}$$

Where $\hat{Y}$ denotes the predicted value. $X_1, \cdots, X_p$ are the predictor variables and $\hat{\beta}_0, \cdots \hat{\beta}_p$, the coefficient estimators. Y Denotes the actual value of S_r which is the predicted value together with an error term ϵ. The predictor variables are estimated by minimizing the residual sum of squares (RSS) which is representative for the error term. In Figure 2.9 a 2-variable representation of the minimization of RSS is illustrated. The plane is positioned in such a way that the sum of the errors (black lines) is minimized.

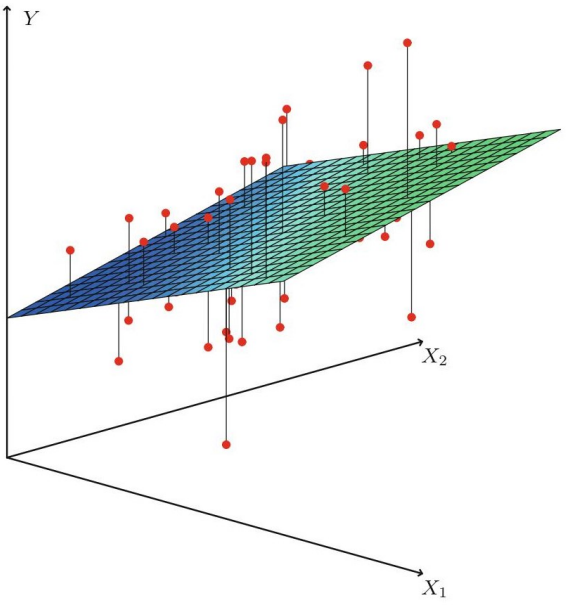

Figure 2.9: Visualisation of a plane describing the least-square fit to a dataset. Where the distance between the data points is minimized for a N-dimensional plane. Note reprinted from: (Gareth James, Daniela Witten, Trevor Hastie, 2013, pp. 73)

The selection of the predictor variables for the regression model is commonly achieved via the following methods: stepwise forward selection, stepwise backward selection and a best-subset selection. Forward selection starts with a null mode, merely containing an interception constant. Next, the variable resulting in the lowest RSS is added to the model. This process continues until all variables are added or another stop condition is met. Backwards regression starts with all variables and removes the least significant variable. Best-subset regression assesses each possible combination, 2^p combinations, which is computational demanding. However, in applying the best-subset method the order of the different predictor variables is not relevant. Therefore, no combination of variables is missed. Despite the computational constraints, the best-subset approach is applied in this research. A selection with the help of a PCA is not only reducing the risk on multi-collinearity, it also reduces the demand of computational time.

2.5.2. Variable selection

A Principal Component Analysis (PCA) will be performed to get more insight into the different predictor variables and their relationships. Moreover, the PCA could be used to reduce the dimension of a datasets feature space. This prevents any collinearity and obviate over-fitting in regression analysis. This feature reduction will be performed by plotting the loadings of the different compared predictor variables on the first two principal axes, one could graphically grasp the correlations between the different predictor variables. The direction of the loadings will indicate the relationship between the predictor variables. Based on the results of the PCA, a selection is made to perform the regression analysis.

The best-subset method is comparing models containing various amounts of predictor variables. Therefore, it is necessary to find the optimal amount of variables for the regression model. To achieve this, the performance of models containing different amount of variables are compared to ensure no over-fitting is occurring. The models are assessed using R^2 and R^2_adj and leave-one-out cross-validation (LOOCV). Application of a LOOCV is common when lacking sufficient data to split the dataset between a test and training set. With LOOCV, one data point is used to validate the training set of all the remaining data points. The process is repeated until every data point is used for validation (Gareth James, Daniela Witten, Trevor Hastie, 2013). In practice, different definitions of R^2 and R^2_adj are used, these metrics are defined in this study in 2.17 and 2.16.

An Exhaustive feature selection algorithm is used to evaluate the subset of features (Raschka, 2018). The best 5 models are selected for each number of variables in a subset. The selection is based on the LOOCV score to find the optimal amount of variables used to examine the model variables. If abundant variables are added to the model, the LOOCV will decrease and over-fitting is occurring. After the model selection, the coefficients of these best performing models are investigated.

$$R^2 = 1 - \frac{SSR}{SST} \tag{2.16}$$

$$R^2_{adj} = 1 - \left(1 - R^2\right)\left[\frac{n-1}{n-(k+1)}\right] \tag{2.17}$$

Where SSR is defined as the sum of squares of the residuals and SST as the total sum of squares. Where n is the sample size and k is the number of independent variables in the regression equation.

2.6. Regression variables

The multiple linear regression is performed using land cover and climate variables. In this section, these 2 groups, expected to influence S_r are discussed. The variables are explained and their use for this study is substantiated.

2.6.1. Land cover classification

To observe the effect of vegetation on S_r, a land cover classification is required. The classification is based upon the land cover dataset of the climate change initiative (CCI) (European Space Agency and Climate

Change initiative, 2014). This dataset has global coverage for the period 1992-2015 with a 300 meter spatial resolution and a yearly temporal resolution. The CCI dataset results from a machine-learning algorithm, compiling from different satellite data products. The vegetation type is the predominant factor in the land cover classification dataset and therefore assumed to be a good indicator to find a relationship between vegetation and the rootzone storage volume. For every catchment, the coverage percentages of the land cover types are calculated with a zonal statistics tool. Resulting in a time-series of land cover fractions for the period 1992-2015. To reduce the number of land cover variables, 3 different categories were compiled according to the IPCC classification in the supporting documents (UCL-Geomatics 2017, 2017). The three categories are forest, grass and cropland. Each category is expected to represent a different size of S_r corresponding to the key survival strategy of the ecosystem.

2.6.2. Climate variables

To observe the effect of long-term climate effect on S_r, climate indicators are determined. In this section, the indicators for which we expect to influence the rootzone storage capacity are discussed. First general climate indicators are discussed, afterwards the snow dynamics indicators are described.

Run-off coefficient

The study of Gao et al. (2014) showed a noteworthy negative relationship between the run-off coefficient (RC) and S_r. RC is defined as the long-term fraction of precipitation resulting in run-off, see Equation 2.18. According to the author of the article, this relationship could indicate that an increasing RC, the water available for actual evaporation is decreasing. This means that less transpiration will occur, and this could lower the storage needs of the vegetation. RC represents the geographic properties along with the vegetational properties of the catchments.

$$\mathrm{RC} = \frac{\overline{Q}}{\overline{P}} \tag{2.18}$$

Seasonality index

Seasonality of precipitation seems an important driver in the development of the rootzone storage. Since the seasonality describes how the precipitation input is distributed over a year. If there is low seasonality, there is a higher chance that there will shorter periods of droughts and therefore more likely to have lower storage deficits. Walsh and Lawler (1981) introduced a metric to quantify the seasonality of rainfall, the seasonality index, see Equation 2.19. For this research, rainfall is not the only inflow of liquid water into the rootzone storage. Snowmelt is another crucial source of liquid water. Therefore, in the original equation, precipitation is substituted with the sum of snowmelt and rainfall as defined in 2.20.

$$\mathrm{SI} = \frac{1}{\overline{P}_{liq}} \sum_{n=1}^{n=12} \left| \bar{\mathrm{x}}_n - \frac{\overline{P}_{liq}}{12} \right| \tag{2.19}$$

Where SI is the seasonality index, $\overline{P}_{liq}$ the mean annual liquid water input and $\bar{\mathrm{x}}_n$ the mean rainfall of month$n$.

$$P_{liq} = P_e + M \tag{2.20}$$

Aridity index

The aridity index as defined in Equation 2.1, is used to assess the aridity of the catchment and indicates if the evaporation in a catchment is limited by water shortage or limited by the energy input. The aridity index could also indicate the risk on a long period of drought which could influence the rootzone storage capacity. Therefore, the Aridity Index is included as a possible exploratory variable.

Phase lag

As described by De Boer-Euser et al. (2019), the difference between the timing of liquid water supply and demand of vegetation via transpiration is assumed to be the most important influencer for S_r. If the timing of liquid water input and transpiration are out of phase, the storage deficit could grow over time and that means that more storage capacity is necessary. Therefore, this phase lag might be an interesting variable to include in this study. The phase lag (ϕ) is calculated by identifying for each year the maximum rolling average of 10 days for liquid water input and potential evaporation. Liquid water input is calculated as the sum of effective precipitation and snowmelt. Afterwards, for every year, the "day of the year" of the maxima is determined. Lastly, the day corresponding to the potential evaporation is subtracted with the day of liquid water input, the results for each year are averaged per catchment. A positive ϕ will thus argue that the precipitation peak occurs before the evaporation peak, and vice versa.

Normalized Difference Vegetation Index

The Normalized Difference Vegetation Index (NDVI) is a valuable indicator for the period of transpiration because it used to estimate plant productivity and for this productivity, transpiration is required. NDVI is detecting the absorption of radiation by plants performing photosynthesis. The ratio between visible red (Red) and the near infrared radiation (NIR) defines the NDVI, as described in Equation 2.21. Snow cover is influencing the absorption by blocking the radiation. If snow cover is occurring, NDVI as an indicator of transpiration is less reliable, therefore not the start of the NDVI increase was chosen but the amount of days per year above a certain threshold, in this case, is chosen for a threshold of NDVI = 0.5, in that way it is ensured that snowmelt is of no influence and the found signals are related to the greening of the understory and the unfolding of the canopy (overstorey). Daily NDVI NOAA/AVHRR data was retrieved and a daily catchment average was calculated. Whereafter for each year, the number of days above this threshold were calculated. A visual representation of this approach can be seen in Figure 2.10.

$$NDVI = \frac{NIR - Red}{NIR + Red} \tag{2.21}$$

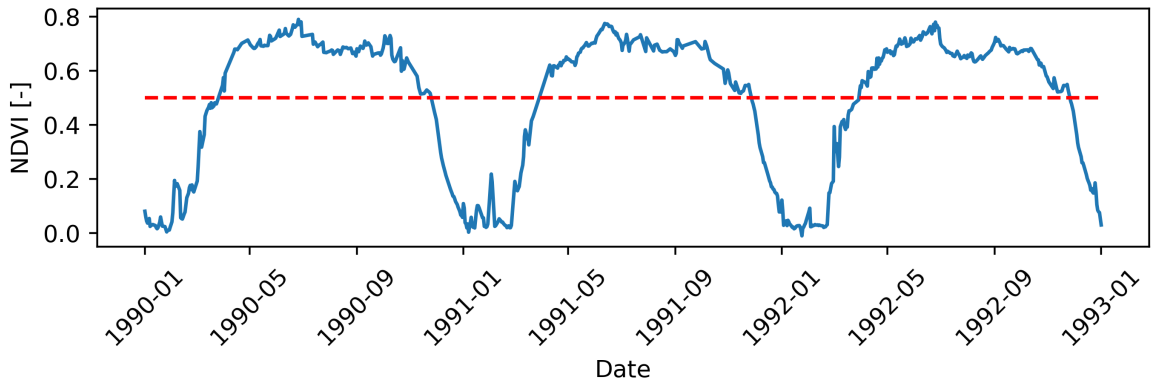

Figure 2.10: The NDVI from 1990-1992 in catchment 204859. The red dashed line indicated the threshold of NDVI = 0.5. The period above this line is measured as indication of the length of the transpiration season.

Slope

Since the growth of roots might be bounded by its physical environment, a representative variable should be included in this study. On steep slopes, it often occurs that only a shallow soil layer is present. In the case, trees manage to grow on these steep slopes, the shallow soil will limit their rooting system. This could significantly influence the maximal rootzone storage capacity created by these trees. Therefore, it is convenient to include the slope as an indicator for root growth limitation. The slope in the catchment was obtained from a raster file with a spatial resolution of 25 meter (European Union, Copernicus Land Monitoring Service 2020, 2020). To obtain the slope in degrees, a conversion was necessary. For every catchment the average slope was calculated with the help of zonal statistics, averaging the pixels values within the catchment.

Snow

Snow is an import precipitation element in Austria. Moreover, snow cover is creating a time-lag in the water input available for transpiration. De Boer-Euser et al. (2019) found that this time-lag could have an influence on S_r. Therefore, multiple predictor variables related to snow and its timing are included. Firstly, the snow-off day is calculated. This is done by finding for every year the highest snow peak in the first half of the year. The first day of a period of 7 days without snow after this peak is defined as the snow-off day of that year. A similar method is applied for the snow-on day, the first day of a period of 7 days having snow cover, in the second half of the year.

Another promising predictor variable is the (non-)coincidence of the snow-off and onset of potential evaporation. As discussed this (non-)coincidence has shown to have a large effect on the rootzone storage. This could make sense since early snowmelt increases the time-lag with the onset of transpiration and could increase a storage deficit. Since the potential evaporation data was sporadic greater than zero during the beginning of the year, a threshold was assumed to be the onset of the potential evaporation. This means, it is assumed that if the potential evaporation reaches a 10% of its maximal value, that corresponding day is defined as the onset day of potential evaporation.

2.7. Temporal analysis

Vegetation can dynamical adapt its rooting systems and therefore its rootzone storage (Gentine et al., 2012). Therefore, vegetation can react to developments within its ecosystem. These changes are perchance more abrupt human-induced land cover change e.g. forest clear-cutting or a more gradual natural development of the ecosystem. This gradual change can be indirectly anthropogenic induced as well through climate change. Using a temporal analysis it is attempted to identify if the rootzone storage is varying. The cause of this change can be explored accordingly. The CCI land cover dataset has an overlapping period of 17 years with the hydrological dataset. Therefore, the dynamic behaviour could only be studied in this time-frame.

2.7.1. Moving window

S_r and most climate variables could only be reliably estimated for longer time-series. Therefore, a 10-year moving window method is applied. The period of 10 years is long enough to smooth out extreme years and short enough to observe a trend. However, the moving windows are not suitable in the multiple linear regression analysis since a strong correlation between the consecutive windows is expected. Therefore, a stationary window is used for the temporal regression analysis.

2.7.2. Stationary window

Although S_r could be estimated based on the year before the land cover change. Nijzink et al. (2016a) used a window of 2 years for calculating S_{r1} to study the change of rootzone capacity. In the described study, the system changed drastically because of deforestation, resulting in a more dynamical adaptation of the rootzone. On the contrary, it is expected that in this study, catchments will not experience major changes in land cover. The rootzone is expected to be less dynamically adapting to the land cover change. Therefore, a longer window of 5 years is used.

This 5-year window is however not of sufficient length to reliably estimate S_{r20}. Hence, S_{r10} is used in this case. 4 windows of 5 years are created for the land cover, the window starts in 1987 and the corresponding land cover values are chosen based on the end of the window. Accordingly, one could observe if the change in S_{r10} is visible in the land cover fractions as well. The 4 windows will be used in multiple linear regression.

3

Results

In this chapter, the results will be reported and discussed. In Section 3.1, the calibration results will be presented. Section 3.2 will discuss the estimated predictor variables. The results of the data selection and the consecutive regression analysis will be discussed in Section 3.3. The results of the temporal regression analysis will be on elaborated in Section 3.4.

3.1. Calibration result

A calibration was performed on a period from summer 2001 until the summer of 2006. The validation is performed for the period of summer 2006 until summer 2008. From the calibration, the 10 best performing combinations of C_m and T_{tr} were selected and used in the validation process. The combination performing best for the combined calibration and validation was selected for each catchment.

The calibration was performed for various amounts of accepted cloud cover for the detection of snow cover, as discussed in Section 2.4. The compared maximal accepted cloud cover percentages were: 50, 60, and 70 percent. The fraction of days, for which the snow cover does not correspond with the calibration and validation, is determined for each elevation. As one can observe in Figure 3.1, the 50% allowed cloud cover is performing best, considering the amount of non-matching days. However, the difference with 60% allowed cloud cover is minimal. The performance is described as the amount of non-matching days divided by the total days without cloud cover. A mean percentage of 4% for the 50% case, is an acceptable performance. One should take into account that this percentage is influenced by the fact that all days of the year are included in the calibration. This means that the relevant performance is slightly worse than the displayed results. With the selected values for C_m and T_{tr}, the snow-dynamics in the model can be estimated.

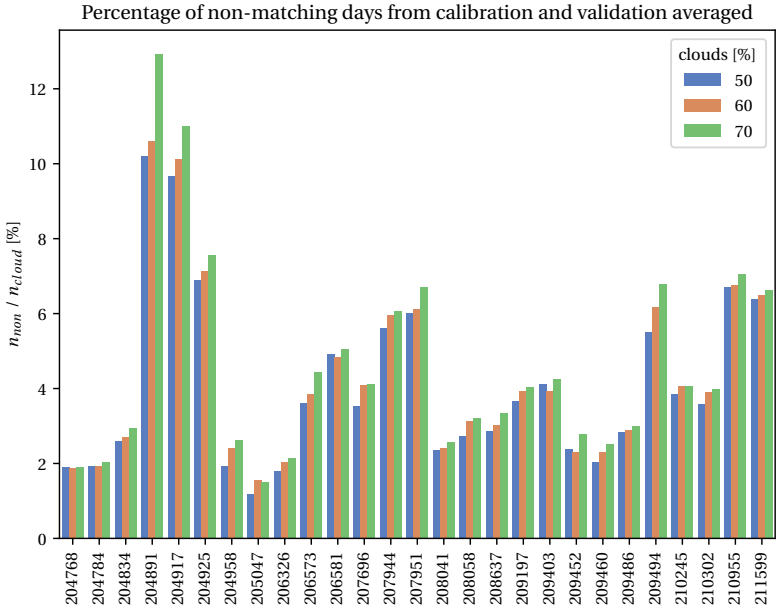

Figure 3.1: The result of the combined calibration and validation process for all catchments. The performance is described as the amount of non-matching day (n_{non}) divided by the total cloud free days ($n_{cloudfree}$). (n_{non}) is defined as the amount of non-matching days between the modelled snow cover based on a combination of threshold temperature and melt factor, with the observed snow cover. ($n_{cloudfree}$) is defined as the total observed days without cloud free days. The result of the best performing combinations of C_m and T_{tr} is presented for every catchment.

3.2. Derivation of variables

To perform regression analysis, the variables are derived based on different datasets. First, the results of the derivation of S_r will be presented, and the result for S_r of the iterated catchments will be evaluated. The resulting land cover and climatic variables will be presented.

3.2.1. Derivation of S_r values

Following from the S_r calculations for all catchments is a diverse range S_r values. The rootzone storage capacity lies between 87—275 mm. On the map of 3.2, one could see the distribution of S_r over the different catchment in Austria. The higher values are located in the (north) east of Austria. The lower values are situated more central North, but here is more variation in the values of S_r. So, there is some clustering visible, however not enough to observe a clear pattern is in the spatial distribution of S_r. In Appendix C.1, a table with the different return periods is provided.

3.2.2. Iterative correction

The processing of data is a substantial part of this research. During the processing, insights were created and decisions were made. As discussed in 2.1, the initial dataset of 69 catchment was reduced to 27 catchment, due to limitation of the data quality, times-series length and suitability for the research. 6 Catchments were corrected using an iterative approach. However, those 6 catchments resulted in untrustworthy coefficients from the multiple linear regression for the temporal case. Likely a result of the fact that the iterative correction method lowers the transpiration in years there is not enough water to full-fill the transpiration needs of the vegetation. This surplus of transpiration is therefore distributed over the other days of the year to full-fill the closure of the water balance. Which leads to a shift in storage deficit. Subsequently, it could happen that via the static window procedure, S_r is calculated inaccurately for these smaller windows. Resulting in mistaken coefficients in the regression analysis of Section 3.4.

Performing the regression analysis showed a negative coefficient for the Aridity Index. This seems not plau-

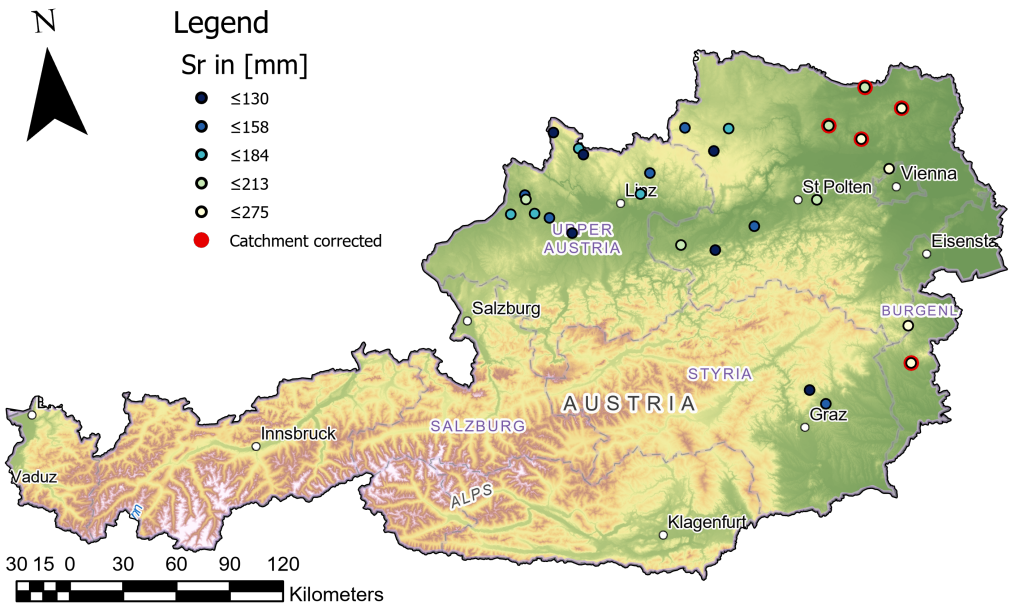

Figure 3.2: S_r for 27 catchments across Austria. The red outline indicates the corrected catchments, excluded from the regression analysis. If a more blue indicates a lower storage deficit. The highest storage deficits are situated in the eastern part of Austria.

sible in reality since a higher Aridity Index is initiated when there is less precipitation input. While E_p is more constrained by the energy input which is related to its geographical location and is normally a more constant factor than precipitation. Thus, it seems not plausible that an increasing Aridity Index is resulting in decreasing rootzone storage.

Exploring the possible cause of this unlikely relationship, it was observed that leaving out the iterative corrected catchments resulted in a non-negative coefficient for the Aridity Index. Such a relationship is plausible. The catchments used for the regression analysis are therefore reduced to 21 catchments.

The applied iteration method is suitable for the correction of the transpiration when the results are analysed afterwards for a full time-series. However, when one is examining parts of the time-series, the reallocation of transpiration is influencing the results on a smaller time-scale. This means that when the full time-series is split into different windows, this can cause a non-reliable estimation of S_r in the different windows.

3.2.3. Climate variables

The climate variables are initially calculated over the full time-series of the data, the selected variables are displayed in Figure 3.3. Interesting to see in Figure 3.3a is that the spread of the Run-off coefficient and Aridity Index is substantial. All catchments are energy limited based on the Aridity Index. In Figure 3.3b it is important to notice that values of the phase-lag (ϕ) between the precipitation peak and evaporation peak are close to zero. This means that the timing of the water supply coincides with the atmospheric demand. An overview of the calculated variables can be found in Appendix D.

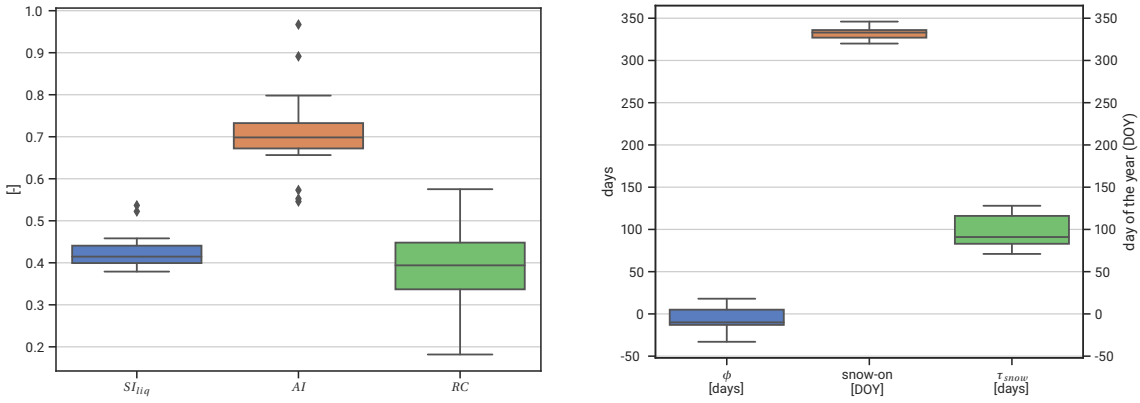

(a) (b)

Figure 3.3: Overview of the climate variables. (**a**): The variables: SI_{liq} , AI, RC, note that the variables not have the same quantity however all are unit-less. (**b**): ϕ', 'τ_{snow}','$snow-on$', note that in this sub-figure the quantity for ϕ and snow-on is: 'day of the year' and for τ_{snow}: a period of days

3.2.4. Land cover variables

In Figure 3.4, land cover seems rather clustered across Austria, with regions of high cropland cover are especially present in the north-east and north-west. No catchments have a majority of forest land cover. Catchment having a majority of cropland cover, do not have substantial forest land cover. The agricultural areas seem to be logically situated on the lower elevated regions.

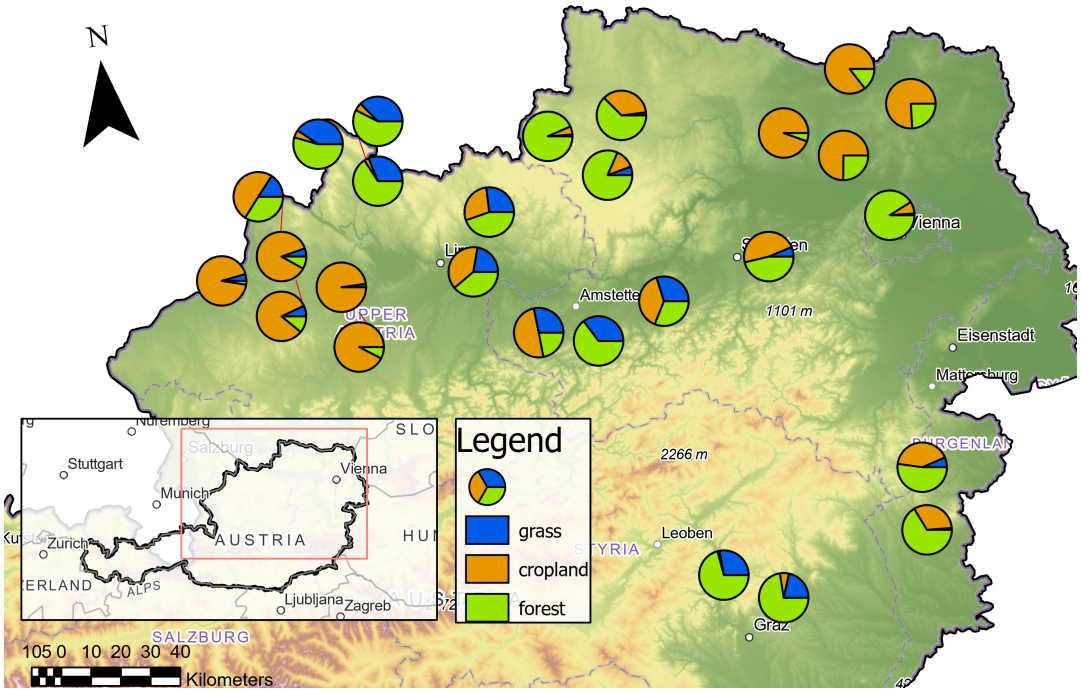

Figure 3.4: The different land cover fraction per catchment, showing a variety in catchment compositions, agricultural catchments are noticeably clustered.

3.3. Spatial analysis

Before the regression analysis can be performed a selection of the variables from Section 3.2.2 has to be made, to prevent from the occurrence of multicollinearity and to lower the computational burden of the best-subset method. A PCA is used to select these predictor variables variables.

3.3.1. PCA

A first step into the variable selection was made with the help of a principal component analysis (PCA). The PCA shows a correlation between different predictor variables. To prevent strong collinearity in the multivariate regression model, a first variable selection is made. This is achieved by selecting a single variable, given that correlated variables describing similar catchment characteristics or processes are present. For example selecting (τ_{snow} for representing the different snow variables). The principal component analysis was performed including the calculated climate variables and the relevant land cover types. The result of this variable reduction is displayed in Figure 3.5. The Figure shows the loadings and directions of the predictor variables in the frame of the two first principal components. Figure 3.5a Shows multiple strong correlations between variables describing the same process. For example, the snow-related variables are all similarly related to S_r.

The total explained variance of PC1 en PC2 in Figure 3.5a is 63%, for the PCA in Figure 3.5b the explained variance is 73%. This means that for both figures not all variance is described by the PCA, however, a substantial part is described and therefore suitable to form a selection for the regression analysis. Interesting to see, is the fact that forest and cropland are orthogonally placed in respect to S_r. This indicates that no strong relationship is expected in the regression analysis.

Correlation of loadings was not the only selection criterium. Some variables are directly describing S_r or seem to explain not as much variance e.g. (τ_{NDVI} and the NDVI onset (the day of the year passing NDVI = 0.5). Moreover, a combination of variables is included and can represent the combination of both variables. A selection of 9 variables is the result of the reduction performed with the interpretation of the PCA. This selection is rather small since in this way the occurrence of multicollinearity is prevented. An overview of the studied variables can be found in Appendix E.

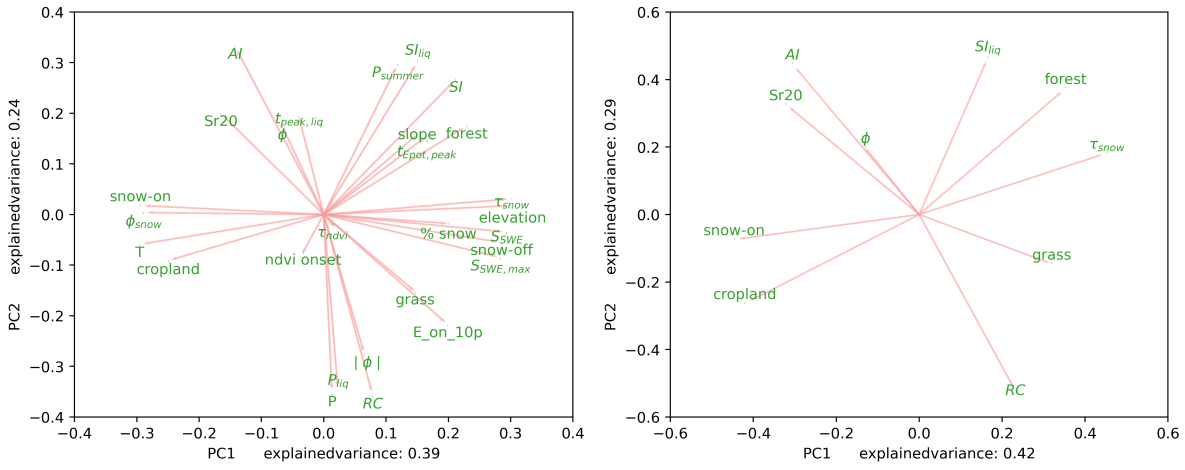

(a) (b)

Figure 3.5: Principal Component Analysis including catchment characteristics and S_r. (**a**) Loadings of all catchment characteristics studied on PC1 and PC2. (**b**) Selection of loadings based on (a), similar characteristics with similar relationships. The variables used in this figure are defined in appendix D

3.3.2. Regression

The multiple linear regression is performed with the 9 variables resulting from selection via the PCA. The results of the predictor variable selection with the exhaustive search method are summarised in Figure 3.6. Here one can observe the leave-one-out-cross-validation (LOOCV) score, R^2 and R^2_{Adj}. For each subset, containing a different number of predictor variables. The average LOOCV score of the 5 best models is displayed in the graph. Looking at a larger amount of best models is resulting in including models performing considerably worse than the displayed average performance. This would give a distorted view. An overview of the different model metrics for the subsets is shown in Appendix F.

The 3-variable regression models have the highest LOOCV score, of respectively 0.73 and a R^2_{Adj} of 0.80. These values indicate a reasonable explanatory and predictive power. Increasing the number of variables above 3, results in over-fitting because the LOOCV score is decreasing and therefore its predictive power (Gareth James, Daniela Witten, Trevor Hastie, 2013). Over-fitting is quickly occurring given the small dataset. The 2-variable models are on average performing less than the 3-variable models, with a maximal LOOCV score of 0.58 and an R^2_{Adj} of 0.68, however, these models are still performing reasonably.

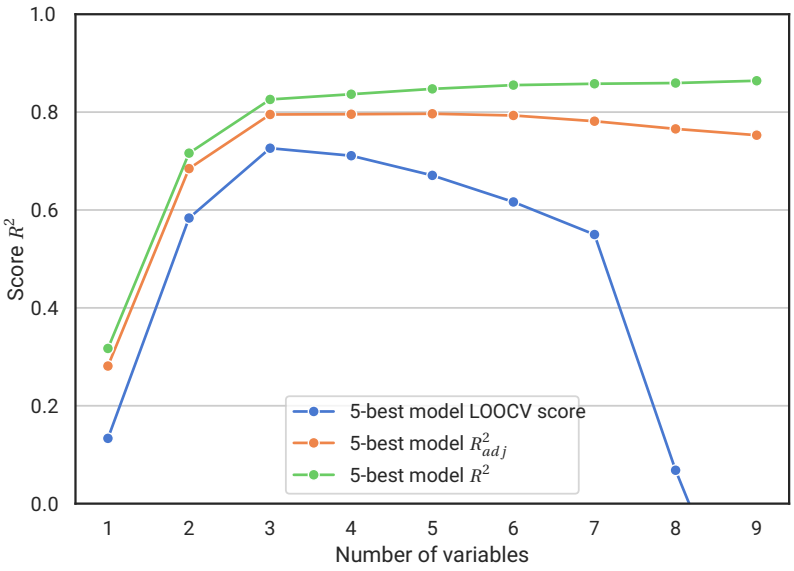

Figure 3.6: Leave-one-out-cross-validation score, R^2 and adjusted R^2 resulting from the multiple regression of the spatial analysis. Based on the LOOCV score, three variables is the optimal model size before over-fitting is appearing. The definition of R^2 and adjusted R^2 is given in Section 2.5.2

Looking at p-values of the different variables in the tables of **??**, it emerges that the there is no combination of a 3-variable model where each p-value is below 0.15 and the Variance Inflation Factor (VIF) is below 5. Above this often use threshold for the VIF it is expected that multicollinearity is occurring (Sheather, 2009). It is hard to declare a cut-off significance level in exploratory research since a too high value could give an inaccurate result and a too low value could dismiss crucial insights.

Following from the selection criteria, a 2-variable model including cropland is therefore excluded. Having a closer look at the remaining 4 best performing 2-variable models, one could observe that the Run-off Coefficient (RC) is present in all 4 models. Furthermore, the variables: SI_{liq},τ_{snow}, %forest and snow-on are present as well, as is shown in Figure 3.7.

The regression coefficient is negative for RC in all models, and the magnitude of these coefficients are the highest. The coefficient of RC is found negative since a high RC indicates a high discharge and by making use of a water balance (eq. 2.6), this high discharge is resulting in low transpiration. The amount of transpiration is critical for the storage deficit and this relates to a high S_r (Gao, Hrachowitz, Schymanski, Fenicia, Sriwongsi-

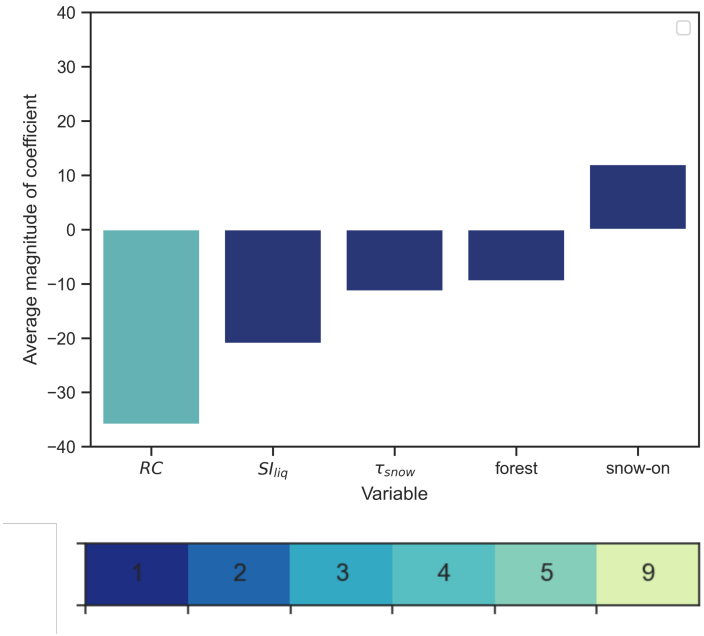

Figure 3.7: The magnitude of the different variables and its occurrences present in the best 4 models resulting from the spatial regression. The colour is showing the number of occurrences of the variable. The y-axis shows the average magnitude of this variable.

tanon, and Savenije, 2014). The magnitude of the coefficient explains its importance since the input data is standardised and likewise the coefficients can be compared.

In addition to the coefficients of RC, the coefficients of the other climate variables are explainable. As discussed in 3.11, ϕ is varying around zero for the studied catchments. A negative coefficient for the seasonality index is in this particular study plausible, since the peak of the precipitation falls during the peak of potential evaporation and thus likely the peak of transpiration. Therefore, a higher seasonality index results in more precipitation during the transpiration peak and therefore less storage deficit is accumulating.

The negative coefficient for the τ_{snow} could be explained as a manner of quantity or as a manner of timing. During the period of snowfall, a higher quantity of snow could be accumulated and therefore more water is supplied at the start of the transpiration season. A longer period of snow cover might therefore lead to lower storage deficits. During periods of snow cover, the amount of transpiration will be minimal. Another explanation could be that a longer snow period indicates that the snow period is ending later in the year. The peak of melt water is consequently more coinciding with the period of higher evaporation.

The positive coefficient for the snow-on day of the year is plausible as well. Since transpiration in this study is scaled with the potential evaporation, which is forced by temperature. The start of the first snow cover of the year is related to temperature. This possibly higher temperature could thus result in a longer period of transpiration and is therefore a opportunity for a higher storage deficit. This temperature dependence seems in agreement with the energy-constrained, relative humid catchments in this study.

In contrast to the climate variables, the observed coefficients of the land cover variables, fractional forest and cropland cover are more difficult to explain based on the literature. A negative coefficient for fractional forest cover is observed. However, considering forests likely have a higher rootzone storage capacity, a positive coefficient is expected (Zhang et al., 2001). Interesting is the fact that in the PCA of Figure 3.5b it is indicated that there is no correlation between these land cover types and S_r. However, the studied combined effect with the Run-off coefficient creates a relationship with S_r. Though, the coefficients for the land cover variables have a lower magnitude than the climate variables and are therefore of less importance in each model. Moreover, the p-values for land cover variables are higher than for the climate variables. Similarly, the positive coefficient for cropland is not expected according to the literature. As for forest cover, the magnitude of the coefficient is lower than the other variables. The last land cover variable not included in the 5 best models is grassland, it is interesting to see that this land cover type seems the least important of the three categories given the fact

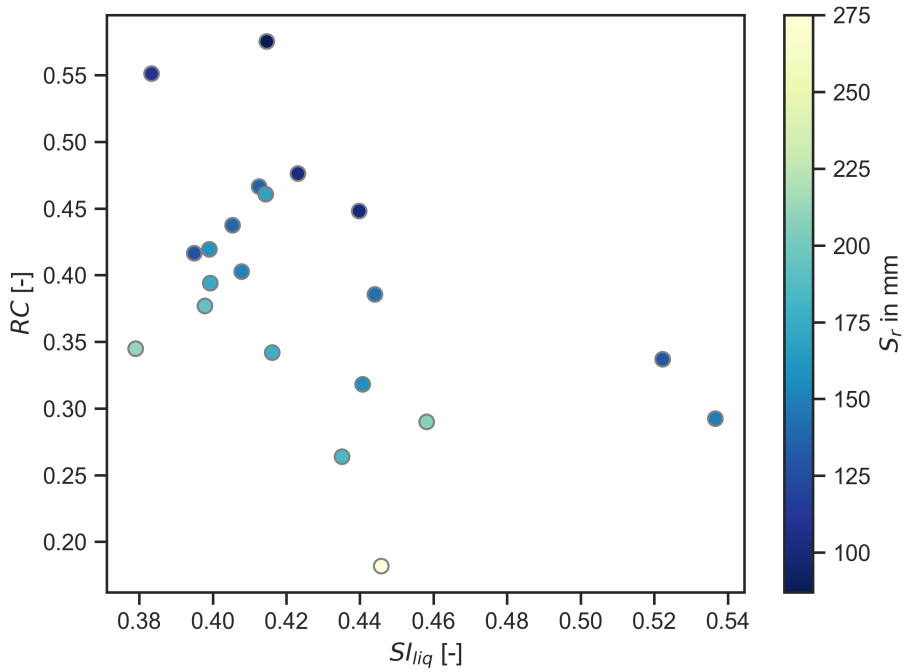

Figure 3.8: A scatter plot showing the Run-off coefficient versus the seasonality index and its corresponding rootzone storage capacity. Visible relationships are in agreement with the sign of the coefficients from the regression analysis.

that its the only fractional land cover variable that showed a correlation with S_r in the PCA.

The regression model of RC, SI_{liq} results in the highest R^2_{Adj} In Figure 3.8 a clear relationship between RC, SI_{liq} and S_r is visible. Where S_r decreases with an increasing RC, together with a decreasing S_r for an increasing SI_{liq}. This observed relationship is similar to earlier described relationships between S_r, RC and SI_{liq}.

Table 3.1: Results of linear regression for the spatial case. The tables show the regression coefficients for the 4 selected models. The VIF and p-value stay below the thresholds set.

(a) R^2_{Adj}: 0.8, LOOCV score: 0.76, F-test :41 , p-value: 1.90e-07. This table contains the best performing 2-variable regression model.

Variable	Coefficient	Standard Error	t-value	p-value	VIF
constant	156.52	4.26	36.72	0.0	-
SI_{liq}	-20.99	4.84	-4.34	0.0	1.29
RC	-43.94	4.84	-9.08	0.0	1.29

(b) R^2_{Adj}: 0.68, LOOCV score: 0.58, F-test :21.83 , p-value: 1.54e-05

Variable	Coefficient	Standard Error	t-value	p-value	VIF
constant	156.52	5.44	28.76	0.00	-
snow-on	12.00	5.60	2.14	0.04	1.06
RC	-31.17	5.60	-5.56	0.00	1.06

(c) R^2_{Adj}: 0.67, LOOCV score: 0.56, F-test :21.35 , p-value: 1.77e-05

Variable	Coefficient	Standard Error	t-value	p-value	VIF
constant	156.52	5.48	28.54	0.00	-
τ_{snow}	-11.34	5.50	-2.06	0.05	1.01
RC	-33.02	5.50	-6.00	0.00	1.01

(d) R^2_{Adj}: 0.64, LOOCV score: 0.51, F-test :19.27 , p-value: 3.35e-05

Variable	Coefficient	Standard Error	t-value	p-value	VIF
constant	156.52	5.68	27.54	0.00	-
RC	-35.58	5.76	-6.18	0.00	1.03
forest	-9.50	5.76	-1.65	0.12	1.03

3.4. Temporal analysis

The box-plots from Figure 3.9 show us the relative change of S_r for all catchment for a period of 26 years (1982-2008). One could observe that the 10-year moving-window method results in an increase of S_r compared with the moving average of the 10 years before 1992. The 10-year moving window results in more smooth behaviour and is intended for the indication of trends only.

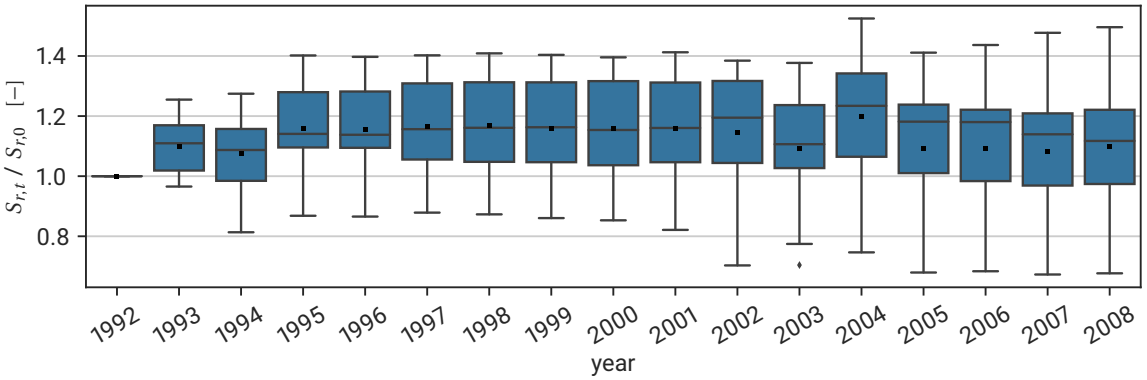

Figure 3.9: S_r change resulting from a 10-year moving-window for the years 1992-2008 compared to the year 1992. An increase in S_r compared to the year 1992 is visible.

The regression analysis from Section 3.3 is performed again, for the same dataset, divided in four 5-year stationary windows for each catchment. The predictor variables are recalculated for each window and displayed in Appendix D.2. A total of 84 data points are acquired in this way. As one could conduct from Figure 3.10 the 4-variable models have the highest LOOCV score before over-fitting occurs. Nevertheless, the performance for all three scores is lower than the result of the spatial case. Resulting in a maximal LOOCV score of 0.52 and R^2_{Adj} of 0.55. In the figure, the LOOCV score is not rapid, but slowly decreasing after it reached its maximum. This slow decrease could result from the occurrence of autocorrelation between the stationary windows. From the 4 and more variable models, the VIF increases above the threshold of 5. The analysis of the coefficients is therefore performed on the 2 and 3-variable models only. The model-selection conditions of 3.3 were applied resulting in 9 models which are analysed further.

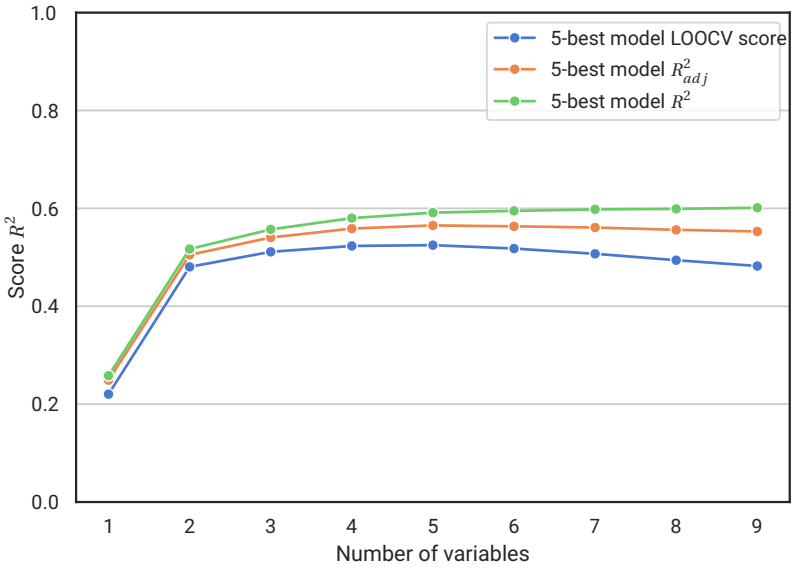

Figure 3.10: Leave-one-out-cross-validation score, R^2 and adjusted R^2 resulting from the multiple linear regression of the temporal analysis. Based on the LOOCV score, 4 variables is the optimal model size however less pronounced as in the spatial case. The definition of R^2 and adjusted R^2 is given in Section 2.5.2

Having a closer look at these 9 models, one could observe that conform the spatial case, the Run-off Coefficient(RC) is represented most. Also, the variables snow-on, % forest, % cropland, and τ_{snow} occurring at least twice. The signs of all variables are consistent and identical to the signs of the spatial regression. This means that the variables are behaving consistently in all models. Figure 3.11 summarises the coefficients resulting from the regression. The corresponding table could be found in Appendix F.2.

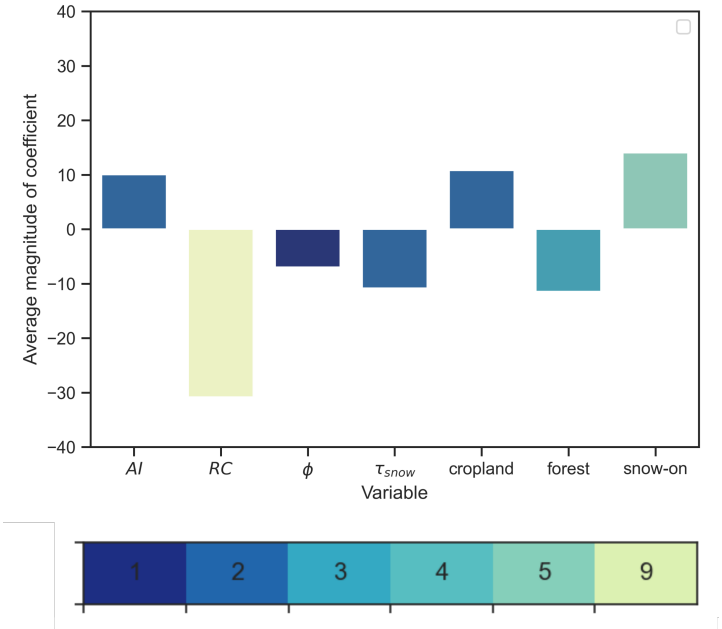

Figure 3.11: Occurrences of variables and its coefficient sign for the best 9 models resulting from the temporal regression. The colour is indicating the times a variable is present in the regression models. The displayed magnitudes shows the average coefficient size when the variable is present.

The importance of RC in the regression models is also visible in Figure 3.12 where an average decreasing trend of RC compared to the year 1992 is observable. This decreasing could be induced by the observed increase of evaporation across Austria, which is related to the increase of global radiation and temperature (Duethmann and Blöschl, 2018).

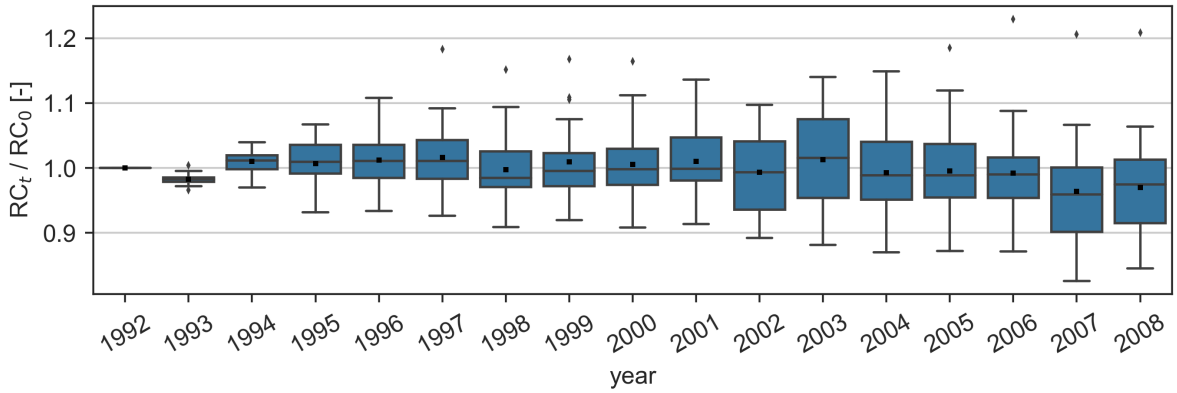

Figure 3.12: Relative change of *RC* resulting from a 10-year moving-average prior to the years 1992-2008 compared to the year 1992. A decreasing trend of *RC* is visible.

The effect of the observed coefficients of the land cover is visible in 3.13. The average total deforestation increased over time however at a low pace. Forest is on average replaced by more grassland than by cropland. However, the differences are small. The observed overall land cover changes are small. A sudden increase of land cover change is visible in the graph from the year 1999. This will be discussed in 4.5.

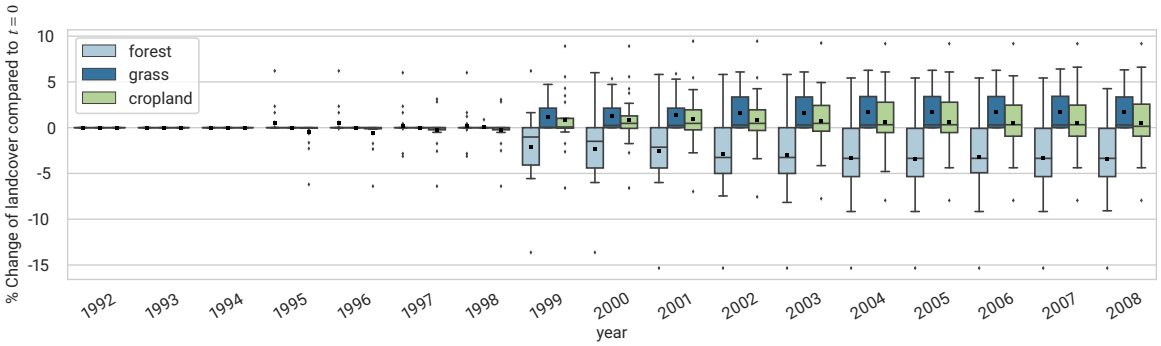

Figure 3.13: land cover change for each year in all studied catchment compared to the year 1992 for forest, grass and cropland as a fraction of the total catchment area. A discontinuity in landcover change is visible.

Introducing the cutting window method does not introduce a clear difference in how different variables describe and predict the change of S_r. However SI_{liq}, is not present in the models and AI and ϕ are new compared to spatial regression. Both are not included in the models often.

Performing the Durbin-Watson test showed the presence of autocorrelation in a major part of the models in this section (Durbin, 1970, Farebrother, 1980). The autocorrelation is introduced using the cutting window method. Since climate and land cover variables changed smoothly, the four windows are correlated to the next window for each catchment.

4

Discussion

In this chapter, the methodology and the reliability of this research are discussed. In Section 4.1 the general limitations of the study and the uncertainties of the datasets are discussed. In Section 4.2 the limitations of the snow cover calibration are discussed. Followed by the model limitations for the determination of S_r in Section 4.3. Section 4.4 discusses the limitations of the regression analysis. Finally, the findings and methods related to the land cover are discussed.

4.1. General limitations

4.1.1. Data

Data quality and quantity are the determining factors for this exploratory research. The potential evaporation, used for the S_r calculations is based on temperature only. This estimation could be enhanced by taking into account other variables. Variables of importance are e.g. wind-speed, air-pressure and solar radiation these can be used with implementing the Penman equation (Penman, 1948). The storage deficit is calculated using transpiration as a ratio of potential evaporation. This simplification could lead to inaccuracy, especially on a small temporal scale as the other described variables can vary significantly. To obtain optimal results for the regression analysis, a substantial amount of data is preferable. However, in this study, a lean amount of catchments is used. Resulting in a higher sensitivity of the results for the characteristics of a single catchment.

Not only the demand side of the water balance suffers from inaccuracies. On the supply-side, precipitation is a common point at issue. The natural high spatial variability of precipitation is a possible cause for inaccuracy in the estimation of storage deficit and therefore S_r.

4.1.2. General

A general point of discussion for this research is the fact that one is comparing S_r with the variables which are both based on the same dataset. This means that there is always some relationship apparent between S_r and the variables present. However, an important difference between the variables and S_r is the fact that S_r is determined from a daily dataset. On the contrary, most variables in this study are long-term statistics and do not always require a daily time-series to be estimated.

In addition to the explored variables, more factors are affecting S_r, omitted variables are inevitable. Plant specific properties are not taken into account, some vegetation have survival strategies which could temporarily minimize the water use of the plant (e.g. grass can get in a state of dormancy). On the supply-side the results could be influenced by high water tables or wetlands, although the fraction of wetlands in this study is negligible.

There is a possibility that the restrictions on catchments based on the assumptions from 2.1 for the climate method, influenced the results. Because catchments supplied by glacier melt were not taken into consideration, these relative humid catchments were not included. Furthermore, the more arid catchments were excluded from the regression analysis since they were more prone to excessive evaporation and multi-year droughts. It follows that the catchment used for analysis were more moderate. This could reduce the representativeness of this study.

4.2. Calibration result

The snow cover is calibrated in such a way that the threshold temperature for ablation and accumulation are the same. In this model, there is no simultaneous occurrence of snowmelt and snow accumulation in an elevation zone. However, both process may occur simultaneously in different elevation zones. In reality, both processes are triggered on different temperatures and simultaneous occurrence of both processes can occur (He et al., 2014).

Since cloud cover is decreasing the reliability of the calibration, a reduction of cloud cover in the data could be attempted. To bring down the number of cloudy days, the MODIS Aqua(MYD10A1) product could be combined with the in this study used MODIS Terra(MOD10A1) (Parajka et al., 2012). Further one could use multi-day snow cover products to reduce the cloud cover.

During the data selection process, most snow-rich catchments were found not to be suitable for this research. Therefore, the snow calibration process did have less impact on the results. Furthermore, due to the lack of these snow-rich catchments, no complete view is given on the performance of the calibration. In this study, it was not possible to study the effect of snow cover extensively. This will have a significant impact on the found relationships.

4.3. Determination S_r

The "infinite reservoir" used in the climate-based model assumes indirectly that roots of the vegetation can grow infinitely. However, the root growth in length and density is likely constrained by different soil types or depth until the bedrock. This limitation could result in a smaller S_r in reality for certain areas . Furthermore, the availability of nutrients could influence the development of rootzone storage.

An important assumption of the climate method is that vegetation exists and given this fact, it is adapted to the climatic conditions. This assumption only holds when there is no influence of anthropogenic activity. In this study, some catchments contained vast amounts of cropland. Cropland is per definition used by human and therefore disturbed. According to the description of the land cover product, the cropland is not irrigated and should have less impact on S_r. Nonetheless, deficit irrigation could be applied during longer periods of drought (Fereres and Soriano, 2007). deficit irrigation could have a major influence on the real rootzone storage deficit. Another point of discussion is that the seasonal collection of crops will prevent vegetation from developing an optimal rootzone.

For this study a homogeneous maximum canopy storage of 1.5 mm was assumed. This assumption of homogeneity is not an adequate representation of reality. Since diverse vegetation have varying capacities for storing water on the canopy. To evaluate the effect and validity of this assumed constant, a sensitivity analysis is performed. In 4.1 the homogeneous base case of 1.5 mm is compared to heterogeneous cases with high I_{max} and Low I_{max}. In both cases the size of I_{max} is different per land cover type and is based upon the land cover in the catchment. For both cases no strong deviation from the base line is visible. Therefore the choice of I_{max} shall not have a big impact on the results.

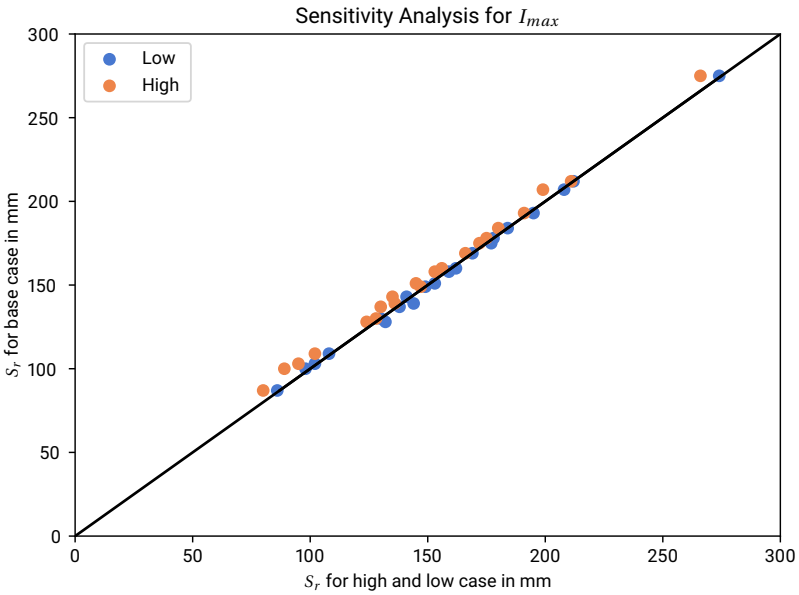

Figure 4.1: Sensitivity analysis for comparing the homogenous I_{max} base case with landcover depending I_{max} for a high and low I_{max} combination. The base case uses a homogenous I_{max} of 1.5 mm. The low case uses 1, 1 and 2 mm for grassland, cropland and forest cover. The high cases uses a combination 1,2 and 4 mm. The choice of I_{max} shows no strong effect on result for S_r.

4.4. Regression analysis

For the regression analysis, the data is standardized to satisfy the assumption for multiple linear regression that the variables are normally distributed. Assumed is, that the relationships between the different variables and S_r are approximately linear. Undoubtedly it is not likely that those relationships are always strictly linear. However, since regression models were able to describe S_r using these linear relationships it is an acceptable assumption to make.

In the field of Earth sciences, all different processes are interconnected. Between hydrology, biology to morphology interconnections arise. This interconnection results in a correlation between the different processes. Multiple linear regression assumes independent predictor variables. Since most processes are at least slightly correlated, this assumption is not strictly met and could influence the results.

Since the amount of 21 studied catchments is rather small, it is not possible to create a separate testing and training subset. Furthermore, the number of training data-points should be ideally larger. In this way, the training and likely the testing score could be more accurate and reliable. Besides, it could create the possibility to predict S_r for the testing dataset.

4.5. Land cover

Chapter 3 showed us that no strong relation was found between land cover and S_r. This could be an artefact of the categorization of the different land cover types in forest, cropland and grassland. The categorization was chosen following the IPCC land categories (UCL-Geomatics 2017, 2017). However, the categorization could have been adjusted to a classification based on a more hydrological perspective.

From the temporal analysis, no influence of importance of the land cover-change on the change of S_r was found. The lack of relationship between the land cover categories is in agreement with the results from the spatial analysis. However, the lack of a relationship could be established by a poor land cover-time-series. In Figure 3.13 is the land cover change in comparison with the year 1992 displayed. The land cover seems to be almost constant until 1999. In the year 1999, there is a sudden increase of land cover change. This sudden increase is likely induced by a change of satellite product were the land cover classification is based upon. In

1999 the AVHHR replaced by the SPOT-VGT product having among other things a finer resolution, 300 meter instead of 1000 meter. Therefore it is likely that minor land cover changes were not observed before.

An observation of landcover change should be first visible at a spatial resolution of 1 km, for the CCI land cover product. Only then the machine learning algorithm of the used land cover product is categorizing at a finer resolution of 300m. Each change has to be present for 2 years in a row to be processed. Therefore a slow degradation or recovery of forest land cover is difficult to observe (UCL-Geomatics 2017, 2017). Furthermore, the accuracy of land cover classified as a mosaic of combined cropland and forest cover has the lowest accuracy. That makes a gradual transition between both types hard to observe.

Comparable to the findings of Bouaziz et al. (2020), the agricultural areas in this study having rather low Runoff Coefficients and a positive relationship with S_r. The relative high silt concentrations at these areas were designated as a possible cause of this positive relationship of cropland with S_r. High concentrations of silt result in a good water-holding capacity of the soil. This high water holding-capacity could result in the fact that it seems cropland grows a relatively large root zone storage capacity. In this study, the regions containing the highest amount of silt in Austria are situated inside the catchments having the higher S_r values as one can observe in Figure 4.2.

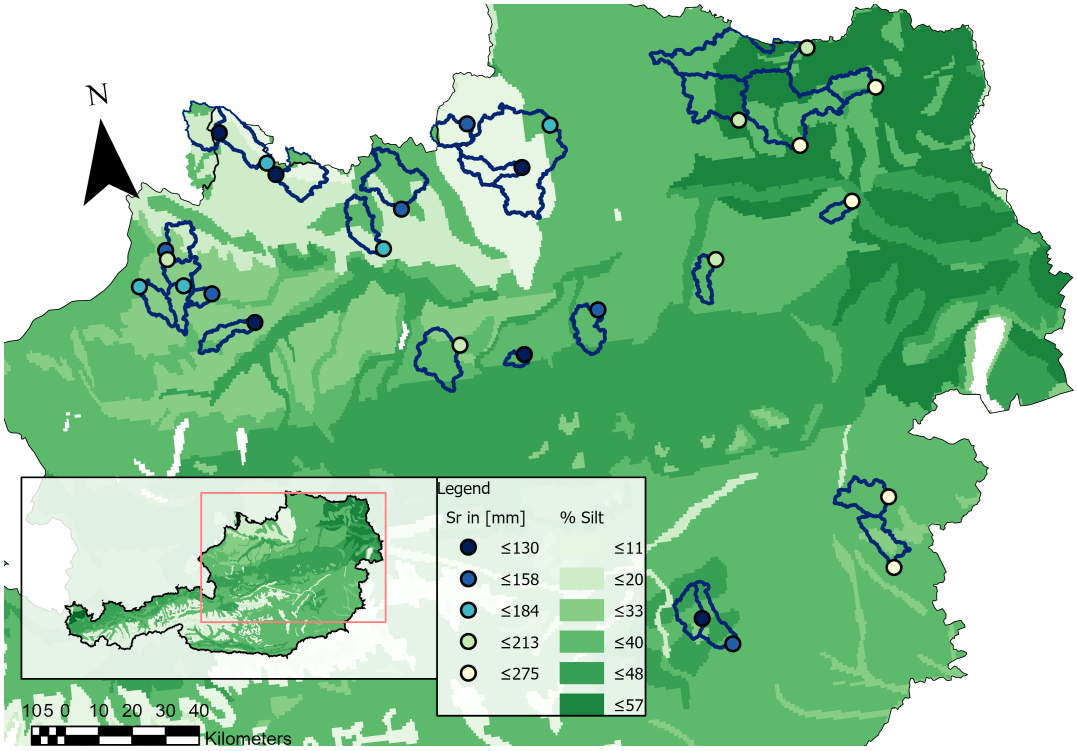

Figure 4.2: The catchments in blue and the data points representing S_r plotted on a map showing the silt fraction as percentage in the topsoil across Austria. The higher S_r values are clearly present at areas containing higher silt fractions. Data is retrieved from the Harmonized World Soil Database (Nachtergaele et al., 2009)

5

Conclusion and Recommendations

The aim of this research was to find a relationship between climatic and vegetational controls, and the root-zone storage capacity in Austria. This study explores spatial and temporal relationships. A MODIS calibrated snow module was added to the conventional model to account for snowfall in Austria. A multiple linear regression analysis was performed to study the different relationships with S_r.

The climate-derived S_r did not show a very strong spatial pattern. However, the highest S_r could be found in the eastern part of Austria. The Northern part had a lower but more varying S_r. In the multiple linear regression the climate variables were most important, especially the Run-off coefficient. The best 5 models were able to describe the behaviour of S_r with an average adjusted R^2 of 0.68. The model which contains the Run-off coefficient and the Seasonality Index performed notably good, with an adjusted R^2 of 0.8. No conclusion could be drawn for the importance of land cover types in the regression analysis, considering the disputable applicability of the land cover data. Furthermore, the coefficients of land cover variables describe behaviour conflicting with the current literature. Though, the found relationships for the land cover variables are weak compared to the climate variables. This weak relationship of land cover with S_r is corresponding with the literature.

This research shows that the rootzone storage capacity changed in the period from 1992 to 2008. On average an increasing S_r was observed for the catchments. However, no strong relationship appeared describing this increase. The regression analysis, both spatial and temporal show the strongest relationship existing between climatic variables and S_r. The Run-off coefficient was the most important variable. Land cover variables were more influential variables in these models as compared to the spatial regression. However due to the sudden shift in land cover in the year 1999, this result is less reliable.

This study shows that it is possible to describe and predict the spatial variability of S_r with long term climate statistics. This study does not claim that this is possible for every type of catchment. Nevertheless, the results could benefit to the prediction of S_r in hydrological similar poorly gauged regions when only long-term climate statistics are available.

Snow dynamics were expected to be of importance during this analysis. Due to the unsuitability of the snow-rich catchments for further analysis the snow dynamics could not be studied extensively. To perceive a relevant view of the variability S_r, these catchments have to be studied as well. The rather small amount of catchment studied in this research resulted in fewer possibilities and higher uncertainty. Therefore, it is recommended for future work to investigate a significantly larger dataset. Since the catchments in this study are rather humid, it would be interesting to investigate in further studies if the found relationships are valid for arid catchments as well. Additionally it would be useful to investigate the unexpected relationship between land cover and S_r further.

A

Python Code: hydrological model

In this appendix a link to a Github repository will be made available. The Github repository will contain the most important Python code for this thesis. The code can be found at: `https://github.com/bartbv/master-thesis`

B

Climate graphs

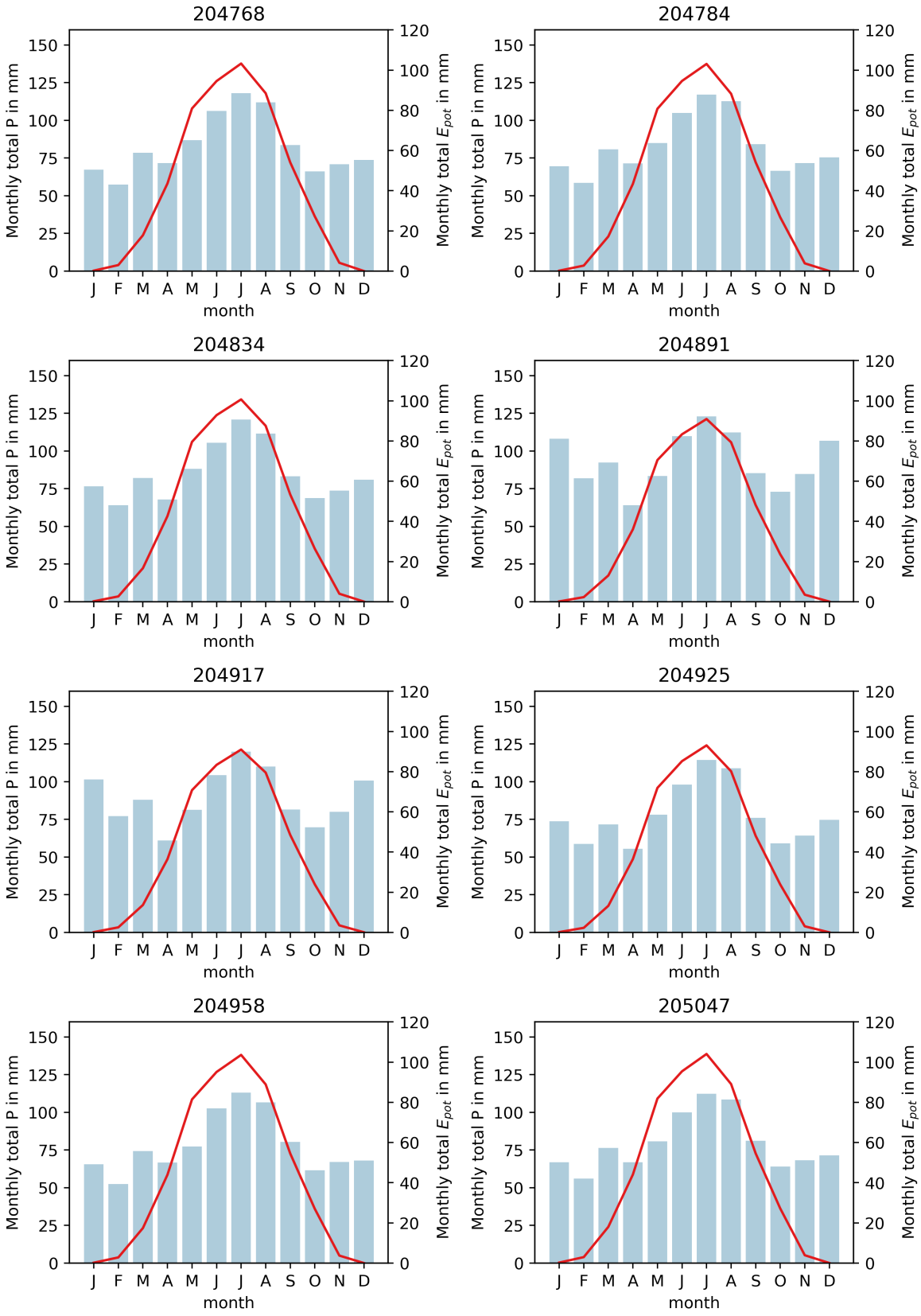

Figure B.1: Climate graphs catchments. Monthly average total precipitation and evaporation, as retrieved from (Gaál et al., 2012)

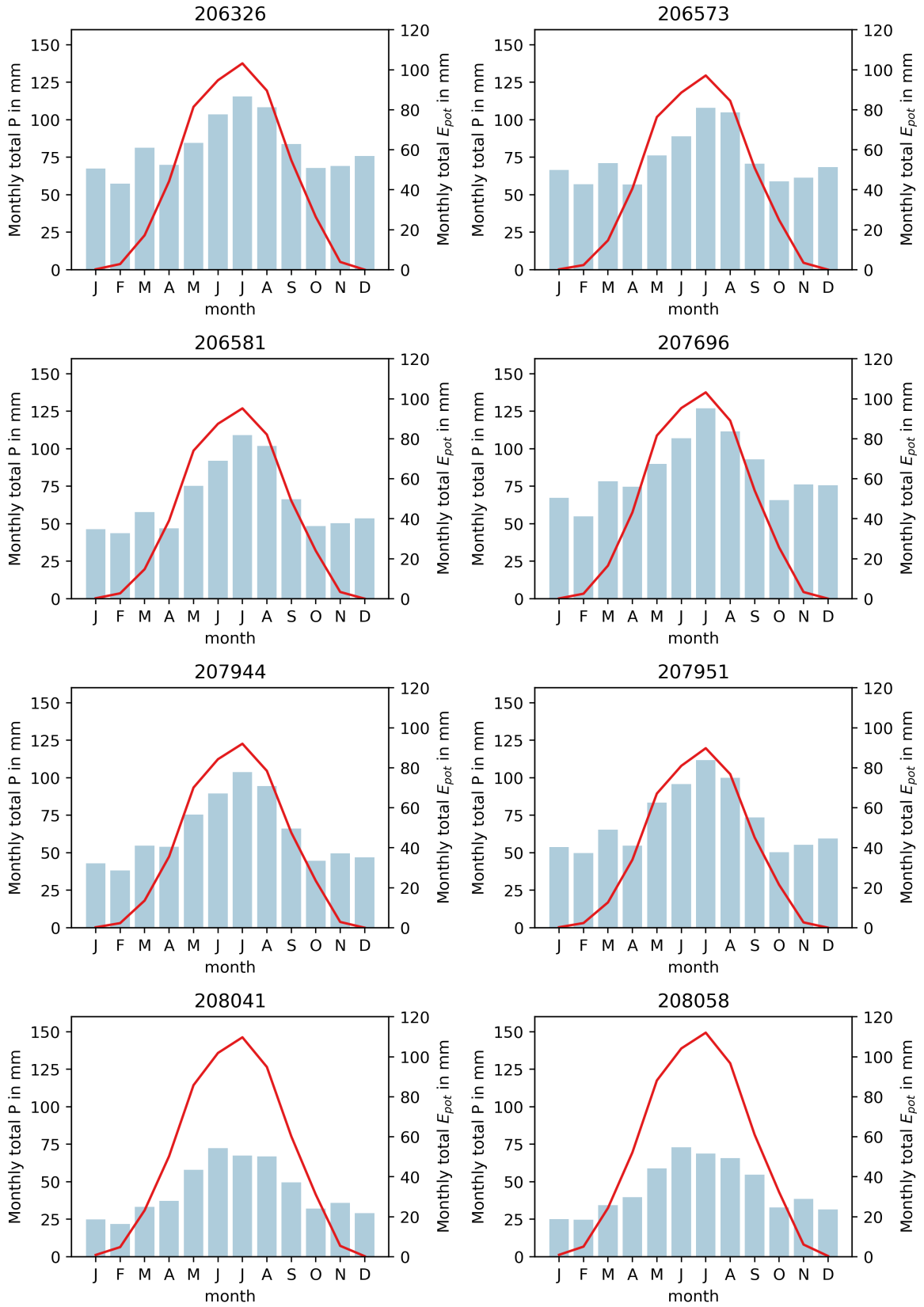

Figure B.2: Climate graphs catchments. Monthly average total precipitation and evaporation, as retrieved from (Gaál et al., 2012)

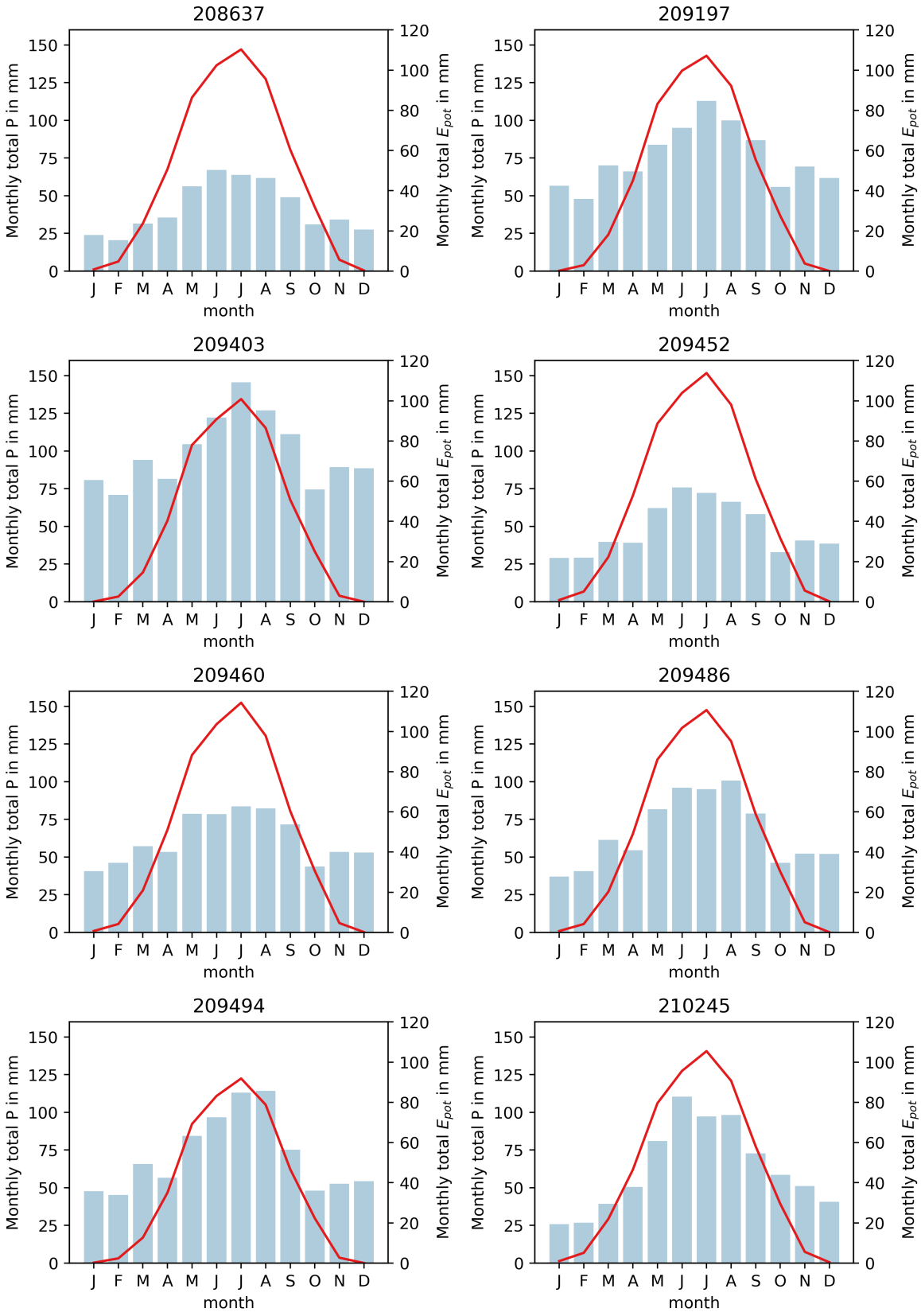

Figure B.3: Climate graphs catchments. Monthly average total precipitation and evaporation, as retrieved from (Gaál et al., 2012)

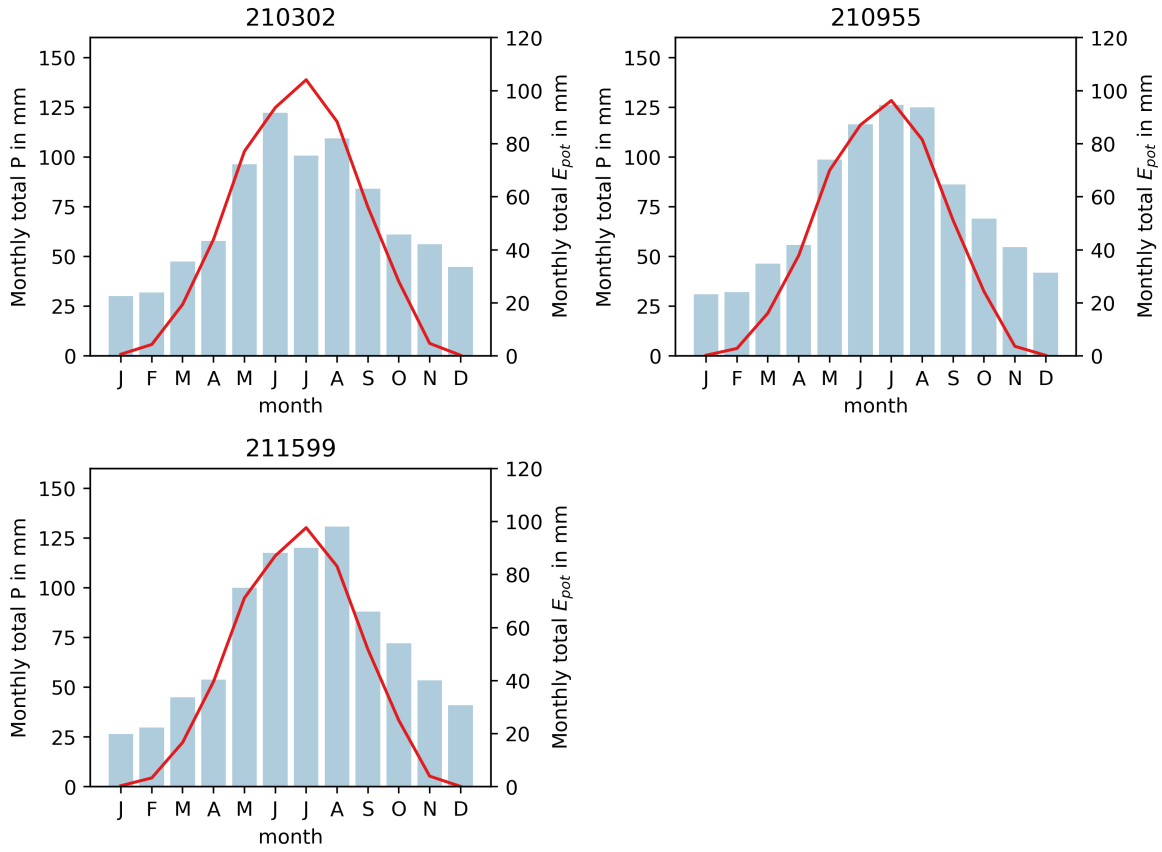

Figure B.4: Climate graphs catchments. Monthly average total precipitation and evaporation, as retrieved from (Gaál et al., 2012)

C

S_r values

Table C.1: Estimated rootzone storage capacities for the return periods of 2,5,10 and 20 years for the different catchments

catchment	$S_{r,2y}$	$S_{r,5y}$	$S_{r,10y}$	$S_{r,20y}$
204768	90	127	151	175
204784	83	116	139	160
204834	72	100	119	137
204891	48	65	76	87
204917	84	121	146	169
204925	57	77	90	103
204958	70	95	112	128
205047	72	101	120	139
206326	98	140	167	193
206573	102	135	157	178
206581	84	116	138	158
207696	117	158	186	212
207944	103	138	162	184
207951	56	75	88	100
209197	82	112	132	151
209403	59	81	95	109
209460	160	210	243	275
209486	109	152	180	207
209494	72	103	123	143
210955	75	99	115	130
211599	85	113	131	149

Table C.2: Estimated rootzone storage capacities for the return periods of 2,5,10 and 20 years for the different catchments

catchment	$S_{r,2y}$	$S_{r,5y}$	$S_{r,10y}$	$S_{r,20y}$
208041	120	160	187	213
208058	133	178	208	236
208637	116	154	180	204
209452	141	195	230	264
210245	122	182	222	261
210302	129	181	216	249

D

Overview calculated climate and land cover variables

D.1. Spatial case

station	snow-on	SI_{liq}	AI	ϕ	τ_{snow}	RC	forest	grass	cropland	S_r
	day of year	-	-	*days*	*days*	-	%	%	%	*mm*
204768	335	0.40	0.69	-14	83	0.39	2.47	4.47	92.78	175
204784	339	0.40	0.69	-12	78	0.42	10.95	7.10	82.63	160
204834	334	0.41	0.66	-12	91	0.47	33.70	15.76	50.01	137
204891	327	0.41	0.55	-11	116	0.58	54.34	40.46	4.94	87
204917	320	0.41	0.57	-10	128	0.46	57.16	37.16	5.17	169
204925	329	0.42	0.66	-5	108	0.48	65.79	31.12	2.96	103
204958	342	0.39	0.73	9	78	0.42	7.53	0.68	91.75	128
205047	340	0.41	0.72	5	71	0.44	0.57	2.13	93.46	139
206326	336	0.40	0.70	-24	83	0.38	8.04	5.38	85.37	193
206573	334	0.42	0.72	-13	95	0.34	37.95	21.80	38.10	178
206581	332	0.44	0.79	-14	103	0.32	43.83	26.48	27.90	158
207696	336	0.38	0.67	10	91	0.34	21.74	27.92	49.32	212
207944	323	0.44	0.80	0	118	0.26	62.17	1.98	35.26	184
207951	322	0.44	0.68	-33	122	0.45	81.48	5.59	12.85	100
209197	333	0.41	0.77	1	90	0.40	30.92	29.71	38.85	151
209403	332	0.38	0.55	-13	88	0.55	64.75	35.25	0.00	109
209460	346	0.45	0.97	-9	86	0.18	87.33	1.16	7.45	275
209486	335	0.46	0.89	18	80	0.29	45.80	6.27	46.94	207
209494	320	0.44	0.70	-19	123	0.39	93.33	1.13	5.42	143
210955	327	0.52	0.70	15	117	0.34	70.71	27.77	1.35	130
211599	327	0.54	0.72	11	109	0.29	72.33	21.54	5.87	149

Table D.1: Selected variables for regression analysis for each catchment

D.2. Temporal case

station	window	SI_{liq}	AI	ϕ	RC	grass	forest	cropland	τ_{snow}	snow-on	Sr
		-	-	*days*	-	%	%	%	*days*	*day of year*	*mm*
204768	0	0.40	0.71	80.4	0.39	4.47	2.23	93.20	53.33	333.0	139.65
	1	0.46	0.66	-12.2	0.42	4.47	2.23	93.20	74.67	325.0	220.11
	2	0.41	0.64	-0.4	0.36	4.47	2.35	92.87	59.33	339.0	161.44
	3	0.43	0.74	-14.4	0.37	4.47	2.79	92.27	106.33	335.0	207.43
204784	0	0.41	0.71	82.8	0.44	7.03	14.38	77.96	54.00	334.0	159.79
	1	0.47	0.65	3.6	0.43	7.03	9.91	82.41	71.67	339.0	193.42
	2	0.41	0.63	12.4	0.38	7.18	7.74	83.65	74.50	334.0	138.80
	3	0.42	0.73	-15.2	0.39	7.14	6.51	84.58	85.00	336.0	181.99
204834	0	0.40	0.70	65.4	0.46	15.76	33.74	50.34	56.67	333.0	158.21
	1	0.46	0.65	-4.6	0.47	15.76	33.74	50.27	77.33	329.0	144.23
	2	0.45	0.61	-20.8	0.46	15.76	33.70	49.89	76.00	333.0	105.24
	3	0.48	0.69	-39.4	0.44	15.76	33.66	49.78	121.67	316.0	139.54
204891	0	0.45	0.57	121.4	0.55	40.21	54.81	4.87	109.33	307.0	82.96
	1	0.45	0.55	7.0	0.58	40.31	54.60	4.93	139.67	305.0	83.21
	2	0.52	0.51	3.4	0.55	40.43	54.30	5.08	112.00	318.0	59.31
	3	0.49	0.56	-40.6	0.52	40.52	54.15	4.92	140.33	313.0	86.22
204917	0	0.46	0.61	70.0	0.47	34.71	60.28	4.80	114.00	305.0	153.39
	1	0.43	0.57	-36.6	0.45	36.70	57.78	5.29	140.00	305.0	162.96
	2	0.54	0.53	-1.6	0.41	38.12	56.05	5.30	116.00	315.0	160.72
	3	0.48	0.58	-36.4	0.43	38.16	55.80	5.14	139.00	312.0	214.91
204925	0	0.49	0.69	43.4	0.43	26.65	71.05	2.31	80.33	322.0	101.90
	1	0.40	0.65	27.0	0.50	29.67	67.63	2.68	97.67	328.0	97.98
	2	0.54	0.62	-3.8	0.47	32.84	63.76	3.27	95.67	329.0	65.26
	3	0.48	0.66	-7.0	0.43	33.24	63.25	3.26	141.33	314.0	76.71
204958	0	0.44	0.77	91.4	0.39	0.68	6.93	92.45	52.33	335.0	142.13
	1	0.46	0.70	-3.4	0.41	0.68	7.86	90.73	75.00	339.0	155.73
	2	0.42	0.67	74.6	0.40	0.68	7.63	89.88	46.67	342.0	109.24
	3	0.40	0.75	-3.2	0.41	0.68	7.63	89.50	85.67	345.0	118.91
205047	0	0.41	0.76	12.2	0.42	2.13	0.47	95.27	52.67	334.0	164.91
	1	0.48	0.68	3.4	0.46	2.13	0.47	94.89	71.67	330.0	160.92
	2	0.42	0.65	46.4	0.44	2.13	0.52	92.91	72.50	334.0	123.05
	3	0.42	0.78	-29.2	0.44	2.13	0.71	91.96	80.00	338.0	155.11
206326	0	0.40	0.73	22.2	0.41	5.34	10.79	82.53	54.33	333.0	202.07
	1	0.46	0.67	4.0	0.37	5.34	6.90	86.31	82.33	329.0	212.30
	2	0.42	0.65	5.2	0.35	5.41	5.91	85.89	65.33	339.0	169.94
	3	0.43	0.75	-40.4	0.33	5.39	5.44	85.90	106.67	335.0	230.76
206573	0	0.50	0.76	37.8	0.33	21.00	38.03	40.43	72.33	330.0	203.43
	1	0.43	0.71	-1.6	0.34	21.72	38.54	38.71	93.67	329.0	156.78
	2	0.51	0.66	25.2	0.35	21.94	38.07	37.14	79.00	335.0	134.95
	3	0.45	0.73	3.0	0.31	22.08	37.66	36.99	137.33	316.0	187.03
206581	0	0.51	0.82	-14.6	0.29	26.10	44.50	28.80	103.67	307.0	149.22
	1	0.45	0.74	1.6	0.33	26.29	44.22	28.62	132.00	305.0	118.70
	2	0.48	0.72	29.2	0.32	26.40	43.87	27.46	78.33	328.0	137.62
	3	0.51	0.81	-28.6	0.30	26.75	43.35	27.23	134.00	314.0	190.89
207696	0	0.44	0.68	57.4	0.34	24.89	27.81	46.88	50.33	338.0	197.59
	1	0.42	0.67	-5.4	0.38	25.93	24.52	49.09	82.67	339.0	229.93
	2	0.43	0.66	-30.2	0.33	28.93	19.33	50.48	71.00	338.0	236.76
	3	0.41	0.68	-24.0	0.34	29.69	18.61	50.16	111.67	339.0	187.20
207944	0	0.51	0.84	-11.4	0.26	1.80	64.09	33.83	89.67	307.0	169.99
	1	0.47	0.77	-21.6	0.28	1.84	63.16	34.61	136.00	305.0	205.55

Continued on next page

station	window	SI_{liq}	AI	ϕ	RC	grass	forest	cropland	τ_{snow}	snow-on	Sr
		-	-	*days*	-	%	%	%	*days*	*day of year*	*mm*
	2	0.49	0.77	-0.4	0.25	2.09	61.37	35.84	102.67	319.0	162.26
	3	0.53	0.76	24.2	0.24	2.09	61.12	36.01	139.67	312.0	200.97
207951	0	0.50	0.71	-2.8	0.44	4.80	83.97	11.15	93.33	305.0	109.65
	1	0.46	0.65	-28.4	0.47	4.96	83.27	11.68	136.00	304.0	66.23
	2	0.50	0.65	-19.0	0.41	6.10	80.18	13.64	113.00	306.0	80.79
	3	0.56	0.66	-48.4	0.46	6.10	79.82	14.00	138.67	312.0	70.42
209197	0	0.49	0.80	-10.0	0.40	24.93	42.53	32.19	71.00	329.0	160.87
	1	0.45	0.76	-16.4	0.42	28.00	34.01	37.64	76.00	325.0	187.05
	2	0.42	0.72	46.8	0.40	30.77	27.19	41.44	85.00	330.0	144.57
	3	0.50	0.73	-22.2	0.40	30.95	27.00	41.37	133.67	314.0	113.82
209403	0	0.47	0.58	9.8	0.59	32.32	67.68	0.00	67.00	333.0	132.05
	1	0.43	0.53	-4.6	0.57	33.60	66.40	0.00	87.67	324.0	119.44
	2	0.41	0.55	-9.6	0.56	35.67	64.33	0.00	73.33	329.0	64.49
	3	0.44	0.51	-29.0	0.49	35.67	64.33	0.00	127.00	314.0	80.41
209460	0	0.60	1.03	-81.8	0.16	1.16	85.23	11.43	36.67	341.0	262.27
	1	0.54	0.90	-16.4	0.25	1.16	88.76	7.36	59.00	342.0	226.18
	2	0.53	0.98	15.6	0.13	1.16	88.33	6.12	49.67	343.0	278.69
	3	0.66	0.95	-4.6	0.16	1.16	87.25	6.01	48.00	339.0	284.78
209486	0	0.57	0.91	-29.0	0.26	6.25	48.36	45.14	52.00	333.0	173.41
	1	0.57	0.87	-7.4	0.29	6.25	46.16	47.01	88.00	325.0	224.40
	2	0.47	0.89	36.6	0.27	6.25	44.79	47.64	53.00	340.0	198.51
	3	0.58	0.84	-42.8	0.30	6.25	44.79	47.45	108.67	320.0	216.98
209494	0	0.47	0.76	-67.6	0.35	1.02	93.90	5.09	108.33	305.0	158.66
	1	0.46	0.63	4.4	0.39	1.11	93.52	5.37	137.33	304.0	106.65
	2	0.50	0.68	-8.6	0.39	1.17	93.08	5.56	100.67	308.0	146.00
	3	0.53	0.68	-10.2	0.44	1.17	93.04	5.56	137.67	312.0	146.85
210955	0	0.55	0.67	-10.0	0.33	24.54	74.23	1.15	92.00	324.0	136.38
	1	0.52	0.69	21.0	0.32	26.65	72.05	1.18	128.67	305.0	103.60
	2	0.55	0.77	11.6	0.31	29.25	69.25	1.22	107.67	326.0	138.11
	3	0.51	0.70	18.8	0.32	29.26	69.00	1.38	148.00	313.0	133.78
211599	0	0.56	0.69	-15.0	0.30	18.16	77.59	4.19	79.67	324.0	159.29
	1	0.53	0.71	45.4	0.29	20.14	74.74	5.00	123.33	305.0	127.54
	2	0.56	0.79	23.0	0.28	23.08	69.86	6.72	87.33	328.0	144.77
	3	0.52	0.72	36.6	0.26	23.20	69.63	6.78	140.00	313.0	182.81

Table D.2: Selected variables for regression analysis based on the windowed dataset for each catchment

E

List of studied variables

Table E.1: Overview of the studied variables in this study. All variables are yearly averages over the entire time-series and catchment averaged. Unless stated otherwise.

Symbol	Explanation
AI	Aridity Index
$t_{peak,liq}$	Day of the year highest liquid water input
$t_{peak,E}$	Day of the year highest evaporation
P_{Summer}	Precipitation in summer
SI_{liq}	Seasonality index of liquid water input
SI	Seasonality index of precipitation
slope	Slope
τ_{snow}	Snow period between snow-on and snow-off
τ_{NDVI}	Period of NDVI above threshold
NDVI onset	Day of the year NDVI above threshold
elevation	Elevation
S_{SWE}	Amount of water equivalent snow cover
$S_{SWE,max}$	Maximum amount of water equivalent snow cover over time-series
E_on_10p	Day of the year that 10% of maximal evaporation is reached
RC	Run-off Coefficient
$abs\phi$	Absolute phase lag between $t_{peak,liq}$ and $t_{peak,E}$ in days
ϕ	Phase lag between $t_{peak,liq}$ and $t_{peak,E}$ in days
P	Total Precipitation
P_{liq}	Total liquid water input
T	Temperature
ϕ_{snow}	Phase lag between E_on_10p and snow-on in days
snow-on	Day of the year that snow is present for the first time
snow-off	Day of the year snow is not for more than 7 days
% forest	Percentage of forest
% cropland	Percentage of cropland
% grass	Percentage of grassland

F

Overview results regression analysis

F.1. Spatial case

F.1.1. Accepted models

Variable	Coefficient	Standard Error	t-value	p-value	VIF	F-test	model-p-value	R^2_{adj}	loocv
Const	156.52	4.26	36.72	0.0	-	41.25	0.0	0.8	0.76
SI_{liq}	-20.99	4.84	-4.34	0.0	1.29	41.25	0.0	0.8	0.76
RC	-43.94	4.84	-9.08	0.0	1.29	41.25	0.0	0.8	0.76

Variable	Coefficient	Standard Error	t-value	p-value	VIF	F-test	model-p-value	R^2_{adj}	loocv
Const	156.52	5.44	28.76	0.00	-	21.83	0.0	0.68	0.58
snow-on	12.00	5.60	2.14	0.04	1.06	21.83	0.0	0.68	0.58
RC	-31.17	5.60	-5.56	0.00	1.06	21.83	0.0	0.68	0.58

Variable	Coefficient	Standard Error	t-value	p-value	VIF	F-test	model-p-value	R^2_{adj}	loocv
Const	156.52	5.48	28.54	0.00	-	21.36	0.0	0.67	0.57
τ_{snow}	-11.34	5.50	-2.06	0.05	1.01	21.36	0.0	0.67	0.57
RC	-33.02	5.50	-6.00	0.00	1.01	21.36	0.0	0.67	0.57

Variable	Coefficient	Standard Error	t-value	p-value	VIF	F-test	model-p-value	R^2_{adj}	loocv
Const	156.52	5.68	27.54	0.00	-	19.27	0.0	0.65	0.51
RC	-35.58	5.76	-6.18	0.00	1.03	19.27	0.0	0.65	0.51
forest	-9.50	5.76	-1.65	0.12	1.03	19.27	0.0	0.65	0.51

F.1.2. Rejected models

Variable	Coefficient	Standard Error	t-value	p-value	VIF	F-test	model-p-value	R^2_{adj}	loocv
Const	156.52	5.82	26.92	0.0	-	18.0	0.0	0.63	0.5
RC	-33.78	5.82	-5.81	0.0	1.0	18.0	0.0	0.63	0.5
cropland	7.78	5.82	1.34	0.2	1.0	18.0	0.0	0.63	0.5

Variable	Coefficient	Standard Error	t-value	p-value	VIF	F-test	model-p-value	R^2_{adj}	loocv
Const	156.52	4.23	37.02	0.00	-	28.39	0.0	0.8	0.75
SI_{liq}	-22.62	5.01	-4.52	0.00	1.40	28.39	0.0	0.8	0.75
RC	-47.28	5.62	-8.41	0.00	1.77	28.39	0.0	0.8	0.75
grass	5.64	4.95	1.14	0.27	1.37	28.39	0.0	0.8	0.75

Variable	Coefficient	Standard Error	t-value	p-value	VIF	F-test	model-p-value	R^2_{adj}	loocv
Const	156.52	4.30	36.37	0.00	-	27.19	0.0	0.8	0.74
SI_{liq}	-23.75	5.97	-3.98	0.00	1.92	27.19	0.0	0.8	0.74
RC	-45.38	5.20	-8.73	0.00	1.46	27.19	0.0	0.8	0.74
cropland	-4.24	5.26	-0.81	0.43	1.49	27.19	0.0	0.8	0.74

Variable	Coefficient	Standard Error	t-value	p-value	VIF	F-test	model-p-value	R^2_{adj}	loocv
Const	156.52	4.39	35.69	0.00	-	25.98	0.0	0.79	0.72
SI_{liq}	-21.03	5.12	-4.10	0.00	1.37	25.98	0.0	0.79	0.72
ϕ	0.15	4.78	0.03	0.98	1.19	25.98	0.0	0.79	0.72
RC	-43.91	5.08	-8.65	0.00	1.34	25.98	0.0	0.79	0.72

Variable	Coefficient	Standard Error	t-value	p-value	VIF	F-test	model-p-value	R^2_{adj}	loocv
Const	156.52	4.37	35.82	0.00	-	26.21	0.0	0.79	0.72
SI_{liq}	-22.23	6.06	-3.67	0.00	1.93	26.21	0.0	0.79	0.72
RC	-44.21	5.02	-8.81	0.00	1.32	26.21	0.0	0.79	0.72
forest	1.92	5.42	0.36	0.73	1.54	26.21	0.0	0.79	0.72

Variable	Coefficient	Standard Error	t-value	p-value	VIF	F-test	model-p-value	R^2_{adj}	loocv
Const	156.52	4.31	36.30	0.00	-	27.08	0.0	0.8	0.71
SI_{liq}	-21.89	5.03	-4.35	0.00	1.36	27.08	0.0	0.8	0.71
AI	-6.84	8.88	-0.77	0.45	4.25	27.08	0.0	0.8	0.71
RC	-50.30	9.59	-5.24	0.00	4.95	27.08	0.0	0.8	0.71

F.2. Temporal case

F.2.1. Accepted models

Variable	Coefficient	Standard Error	t-value	p-value	VIF	F-test	model-p-value	R^2_{adj}	loocv
Const	154.63	3.78	40.96	0.0	-	48.15	0.0	0.53	0.51
RC	-30.98	3.82	-8.10	0.0	1.03	48.15	0.0	0.53	0.51
snow-on	15.96	3.82	4.17	0.0	1.03	48.15	0.0	0.53	0.51

Variable	Coefficient	Standard Error	t-value	p-value	VIF	F-test	model-p-value	R^2_{adj}	loocv
Const	154.63	3.83	40.40	0.0	-	45.75	0.0	0.52	0.49
RC	-35.79	3.87	-9.24	0.0	1.02	45.75	0.0	0.52	0.49
forest	-14.87	3.87	-3.84	0.0	1.02	45.75	0.0	0.52	0.49

Variable	Coefficient	Standard Error	t-value	p-value	VIF	F-test	model-p-value	R^2_{adj}	loocv
Const	154.63	3.85	40.14	0.0	-	44.63	0.0	0.51	0.48
RC	-33.25	3.85	-8.63	0.0	1.0	44.63	0.0	0.51	0.48
cropland	14.16	3.85	3.68	0.0	1.0	44.63	0.0	0.51	0.48

Variable	Coefficient	Standard Error	t-value	p-value	VIF	F-test	model-p-value	R^2_{adj}	loocv
Const	154.63	3.90	39.66	0.0	-	42.61	0.0	0.5	0.48
RC	-31.46	3.95	-7.97	0.0	1.03	42.61	0.0	0.5	0.48
τ_{snow}	-13.25	3.95	-3.36	0.0	1.03	42.61	0.0	0.5	0.48

Variable	Coefficient	Standard Error	t-value	p-value	VIF	F-test	model-p-value	R^2_{adj}	loocv
Const	154.63	4.07	38.00	0.00	-	35.81	0.0	0.46	0.44
AI	13.49	7.00	1.93	0.06	2.96	35.81	0.0	0.46	0.44
RC	-22.55	7.00	-3.22	0.00	2.96	35.81	0.0	0.46	0.44

Variable	Coefficient	Standard Error	t-value	p-value	VIF	F-test	model-p-value	R^2_{adj}	loocv
Const	154.63	3.72	41.57	0.00	-	34.2	0.0	0.55	0.52
ϕ	-7.00	3.79	-1.85	0.07	1.04	34.2	0.0	0.55	0.52
RC	-30.01	3.80	-7.89	0.00	1.05	34.2	0.0	0.55	0.52
snow-on	17.02	3.81	4.47	0.00	1.05	34.2	0.0	0.55	0.52

Variable	Coefficient	Standard Error	t-value	p-value	VIF	F-test	model-p-value	R^2_{adj}	loocv
Const	154.63	3.73	41.49	0.00	-	33.95	0.0	0.54	0.51
RC	-33.03	3.95	-8.36	0.00	1.12	33.95	0.0	0.54	0.51
forest	-8.28	4.72	-1.76	0.08	1.60	33.95	0.0	0.54	0.51
snow-on	10.97	4.72	2.32	0.02	1.61	33.95	0.0	0.54	0.51

Variable	Coefficient	Standard Error	t-value	p-value	VIF	F-test	model-p-value	R^2_{adj}	loocv
Const	154.63	3.74	41.36	0.00	-	33.59	0.0	0.54	0.51
RC	-31.54	3.80	-8.29	0.00	1.03	33.59	0.0	0.54	0.51
cropland	7.46	4.63	1.61	0.11	1.54	33.59	0.0	0.54	0.51
snow-on	11.50	4.69	2.45	0.02	1.58	33.59	0.0	0.54	0.51

Variable	Coefficient	Standard Error	t-value	p-value	VIF	F-test	model-p-value	R^2_{adj}	loocv
Const	154.63	3.76	41.15	0.00	-	32.98	0.0	0.54	0.5
RC	-33.92	3.91	-8.67	0.00	1.08	32.98	0.0	0.54	0.5
forest	-11.27	4.20	-2.68	0.01	1.25	32.98	0.0	0.54	0.5
τ_{snow}	-8.43	4.21	-2.00	0.05	1.25	32.98	0.0	0.54	0.5

F.2.2. Rejected models

Variable	Coefficient	Standard Error	t-value	p-value	VIF	F-test	model-p-value	R^2_{adj}	loocv
Const	154.63	3.78	40.95	0.00	-	32.39	0.0	0.53	0.51
AI	6.55	6.75	0.97	0.34	3.20	32.39	0.0	0.53	0.51
RC	-25.82	6.55	-3.94	0.00	3.01	32.39	0.0	0.53	0.51
snow-on	14.90	3.98	3.74	0.00	1.11	32.39	0.0	0.53	0.51

Bibliography

Laurène Bouaziz, Albrecht Weerts, Jaap Schellekens, Eric Sprokkereef, Jasper Stam, Hubert Savenije, and Markus Hrachowitz. Redressing the balance: Quantifying net intercatchment groundwater flows. *Hydrology and Earth System Sciences*, 22(12):6415–6434, 2018. ISSN 16077938. doi: 10.5194/hess-22-6415-2018.

Laurène J.E. Bouaziz, Susan C. Steele-Dunne, Jaap Schellekens, Albrecht H. Weerts, Jasper Stam, Eric Sprokkereef, Hessel H.C. Winsemius, Hubert H.G. Savenije, and Markus Hrachowitz. Improved Understanding of the Link Between Catchment-Scale Vegetation Accessible Storage and Satellite-Derived Soil Water Index. *Water Resources Research*, 56(3):1–22, 2020. ISSN 19447973. doi: 10.1029/2019WR026365.

Ivano Brunner, Claude Herzog, Melissa A Dawes, Matthias Arend, and Christoph Sperisen. How tree roots respond to drought. *Frontiers in Plant Science*, 6(547), 2015. ISSN 1664-462X. doi: 10.3389/fpls.2015.00547. URL https://www.frontiersin.org/article/10.3389/fpls.2015.00547.

Mikhail Ivanovich Budyko, David Hewitt Miller, and David Hewitt Miller. *Climate and life*, volume 508. Academic press New York, 1974.

Tanja de Boer-Euser, Hilary K McMillan, Markus Hrachowitz, Hessel C Winsemius, and Hubert H G Savenije. Influence of soil and climate on root zone storage capacity. *Water Resources Research*, 52(3):2009–2024, 2016. ISSN 0043-1397. doi: 10.1002/2015wr018115. URL https://agupubs.onlinelibrary.wiley.com/doi/abs/10.1002/2015WR018115.

Tanja De Boer-Euser, Leo Juhani Merio, and Hannu Marttila. Understanding variability in root zone storage capacity in boreal regions. *Hydrol. Earth Syst. Sci.*, 23(1):125–138, 2019. ISSN 16077938. doi: 10.5194/hess-23-125-2019. URL https://www.hydrol-earth-syst-sci.net/23/125/2019/.

Paul A. Dirmeyer, Randal D. Koster, and Zhichang Guo. Do global models properly represent the feedback between land and atmosphere? *Journal of Hydrometeorology*, 7(6):1177–1198, 2006. ISSN 1525755X. doi: 10.1175/JHM532.1.

R. J. Donohue, M. L. Roderick, and T. R. McVicar. On the importance of including vegetation dynamics in Budyko's hydrological model. *Hydrology and Earth System Sciences*, 11(2):983–995, 2007. ISSN 16077938. doi: 10.5194/hess-11-983-2007.

Doris Duethmann and Günter Blöschl. Why has catchment evaporation increased in the past 40 years? A data-based study in Austria. *Hydrology and Earth System Sciences*, 22(10):5143–5158, 2018. ISSN 16077938. doi: 10.5194/hess-22-5143-2018.

J Durbin. An Alternative to the Bounds Test for Testing for Serial Correlation in Least-Squares Regression. *Econometrica*, 38(3):422–429, 1970. ISSN 00129682, 14680262. URL http://www.jstor.org/stable/1909548.

European Space Agency and Climate Change initiative. Quick user guide of the Land Cover State products in GTiff and NetCDF formats. Technical report, European Space Agency Climate Change initiative, 2014. URL http://maps.elie.ucl.ac.be/CCI/viewer/download/ESACCI-LC-QuickUserGuide-LC-Maps{_}v2-0-7.pdf.

European Environment Agency (EEA)" European Union, Copernicus Land Monitoring Service 2020. EU-DEM v1.0, 2020. URL https://land.copernicus.eu/imagery-in-situ/eu-dem/eu-dem-v1-0-and-derived-products/eu-dem-v1.0.

R W Farebrother. Algorithm AS 153: Pan's Procedure for the Tail Probabilities of the Durbin-Watson Statistic. *Journal of the Royal Statistical Society. Series C (Applied Statistics)*, 29(2):224–227, 1980. ISSN 00359254, 14679876. URL http://www.jstor.org/stable/2986316.

Elias Fereres and María Auxiliadora Soriano. Deficit irrigation for reducing agricultural water use. *Journal of Experimental Botany*, 58(2):147–159, 2007. ISSN 00220957. doi: 10.1093/jxb/erl165.

Ladislav Gaál, Ján Szolgay, Silvia Kohnová, Juraj Parajka, Ralf Merz, Alberto Viglione, and Günter Blöschl. Flood timescales: Understanding the interplay of climate and catchment processes through comparative hydrology. *Water Resources Research*, 48(4):1–21, 2012. ISSN 00431397. doi: 10.1029/2011WR011509.

H Gao, M Hrachowitz, S J Schymanski, F Fenicia, N Sriwongsitanon, and H H G Savenije. Climate controls how ecosystems size the root zone storage capacity at catchment scale. *Geophysical Research Letters*, 41(22): 7916–7923, 2014. ISSN 0094-8276. doi: 10.1002/2014gl061668. URL https://agupubs.onlinelibrary.wiley.com/doi/abs/10.1002/2014GL061668.

Robert Tibshirani Gareth James, Daniela Witten, Trevor Hastie. *An Introduction to Statistical Learning*. Springer Science+Business Media New York 2013, 2013. ISBN 9780387781884. doi: 10.1016/j.peva.2007.06.006. URL http://books.google.com/books?id=9tv0taI8l6YC.

Pierre Gentine, Paolo D'Odorico, Benjamin R Lintner, Gajan Sivandran, and Guido Salvucci. Interdependence of climate, soil, and vegetation as constrained by the Budyko curve. *Geophysical Research Letters*, 39(19), 2012. ISSN 0094-8276. doi: 10.1029/2012gl053492. URL https://agupubs.onlinelibrary.wiley.com/doi/abs/10.1029/2012GL053492.

E. J. Gumbel. Probability-interpretation of the observed return-periods of floods. *Eos, Transactions American Geophysical Union*, 1941. ISSN 23249250. doi: 10.1029/TR022i003p00836.

D K Hall and G A Riggs. MODIS/Terra Snow Cover Daily L3 Global 500m SIN Grid, Version 6 , 2016. URL https://doi.org/10.5067/MODIS/MOD10A1.006.

Z. H. He, J. Parajka, F. Q. Tian, and G. Blöschl. Estimating degree-day factors from MODIS for snowmelt runoff modeling. *Hydrology and Earth System Sciences*, 18(12):4773–4789, 2014. ISSN 16077938. doi: 10.5194/hess-18-4773-2014.

Regine Hock. Temperature index melt modelling in mountain areas. *Journal of Hydrology*, 282(1-4):104–115, nov 2003. ISSN 00221694. doi: 10.1016/S0022-1694(03)00257-9. URL https://linkinghub.elsevier.com/retrieve/pii/S0022169403002579.

Manfred Kirchner, Theresa Faus-Kessler, Gert Jakobi, Michael Leuchner, Ludwig Ries, Hans Eckhart Scheel, and Peter Suppan. Altitudinal temperature lapse rates in an Alpine valley: Trends and the influence of season and weather patterns. *International Journal of Climatology*, 33(3):539–555, 2013. ISSN 08998418. doi: 10.1002/joc.3444.

Axel Kleidon. Global Datasets of Rooting Zone Depth Inferred from Inverse Methods. *Journal of Climate*, 17(13):2714–2722, 2004. doi: 10.1175/1520-0442(2004)017<2714:Gdorzd>2.0.Co;2. URL https://journals.ametsoc.org/doi/abs/10.1175/1520-0442{%}282004{%}29017{%}3C2714{%}3AGDORZD{%}3E2.0.CO{%}3B2.

Andrew G. Klein, Dorothy K. Hall, and George A. Riggs. Improving snow cover mapping in forests through the use of a canopy reflectance model. *Hydrological Processes*, 12(10-11):1723–1744, 1998. ISSN 08856087. doi: 10.1002/(SICI)1099-1085(199808/09)12:10/11<1723::AID-HYP691>3.0.CO;2-2.

T E Kolb, K C Steiner, L H McCormick, and T W Bowersox. Growth response of northern red-oak and yellow-poplar seedlings to light, soil moisture and nutrients in relation to ecological strategy. *Forest Ecology and Management*, 38(1):65–78, 1990. ISSN 0378-1127. doi: https://doi.org/10.1016/0378-1127(90)90086-Q. URL http://www.sciencedirect.com/science/article/pii/037811279090086Q.

R. Merz, G. Blöschl, and J. Parajka. Spatio-temporal variability of event runoff coefficients. *Journal of Hydrology*, 2006. ISSN 00221694. doi: 10.1016/j.jhydrol.2006.06.008.

Ralf Merz and Günter Blöschl. A regional analysis of event runoff coefficients with respect to climate and catchment characteristics in Austria. *Water Resources Research*, 45(1), jan 2009. ISSN 00431397. doi: 10.1029/2008WR007163.

P C D Milly and K A Dunne. Sensitivity of the Global Water Cycle to the Water-Holding Capacity of Land. *Journal of Climate*, 7(4):506–526, 1994. doi: 10.1175/1520-0442(1994)007<0506:Sotgwc>2.0.Co;2. URL https://journals.ametsoc.org/doi/abs/10.1175/1520-0442{%}281994{%}29007{%}3C0506{%}3ASOTGWC{%}3E2.0.CO{%}3B2.

Freddy Nachtergaele, Harrij Van Velthuizen, Luc Verelst, Niels Batjes, Koos Dijkshoorn, Vincent Van Engelen, Guenther Fischer, Arwyn Jones, Luca Montanarella, Monica Petri, Sylvia Prieler, Edmar Teixeira, David Wiberg, and Xuezheng Shi. Harmonized World Soil Database. Technical report, FAO, 2009.

R C Nijzink, L Samaniego, J Mai, R Kumar, S Thober, M Zink, D Schäfer, H H G Savenije, and M Hrachowitz. The importance of topography-controlled sub-grid process heterogeneity and semi-quantitative prior constraints in distributed hydrological models. *Hydrol. Earth Syst. Sci.*, 20(3):1151–1176, 2016a. ISSN 1607-7938. doi: 10.5194/hess-20-1151-2016. URL https://www.hydrol-earth-syst-sci.net/20/1151/2016/.

Remko Nijzink, Christopher Hutton, Ilias Pechlivanidis, René Capell, Berit Arheimer, Jim Freer, Dawei Han, Thorsten Wagener, Kevin McGuire, Hubert Savenije, and Markus Hrachowitz. The evolution of root-zone moisture capacities after deforestation: A step towards hydrological predictions under change? *Hydrology and Earth System Sciences*, 20(12):4775–4799, dec 2016b. ISSN 16077938. doi: 10.5194/hess-20-4775-2016.

J. Parajka, L. Holko, Z. Kostka, and G. Blöschl. MODIS snow cover mapping accuracy in a small mountain catchment - Comparison between open and forest sites. *Hydrology and Earth System Sciences*, 16(7):2365–2377, 2012. ISSN 10275606. doi: 10.5194/hess-16-2365-2012.

H Penman. Natural evaporation from open water, bare soil and grass. *Proceedings of the Royal Society of London. Series A. Mathematical and Physical Sciences*, 193(1032):120–145, apr 1948. doi: 10.1098/rspa.1948.0037. URL https://doi.org/10.1098/rspa.1948.0037.

Antonio Roberto Pereira and William Oregon Pruitt. Adaptation of the Thornthwaite scheme for estimating daily reference evapotranspiration. *Agricultural Water Management*, 66(3):251–257, 2004. ISSN 03783774. doi: 10.1016/j.agwat.2003.11.003.

Sebastian Raschka. MLxtend: Providing machine learning and data science utilities and extensions to Python's scientific computing stack. *The Journal of Open Source Software*, 3(24), apr 2018. doi: 10.21105/joss.00638. URL http://joss.theoj.org/papers/10.21105/joss.00638.

H. Jochen Schenk and Robert B. Jackson. The global biogeography of roots. *Ecological Monographs*, 72(3):311–328, 2002. ISSN 00129615. doi: 10.1890/0012-9615(2002)072[0311:TGBOR]2.0.CO;2.

Simon J Sheather. *Diagnostics and Transformations for Multiple Linear Regression*, pages 151–225. Springer New York, New York, NY, 2009. ISBN 978-0-387-09608-7. doi: 10.1007/978-0-387-09608-7_6. URL https://doi.org/10.1007/978-0-387-09608-7{_}6.

M. Sivapalan, K. Takeuchi, S. W. Franks, V. K. Gupta, H. Karambiri, V. Lakshmi, X. Liang, J. J. McDonnell, E. M. Mendiondo, P. E. O'Connell, T. Oki, J. W. Pomeroy, D. Schertzer, S. Uhlenbrook, and E. Zehe. IAHS Decade on Predictions in Ungauged Basins (PUB), 2003-2012: Shaping an exciting future for the hydrological sciences. *Hydrological Sciences Journal*, 48(6):857–880, 2003. ISSN 02626667. doi: 10.1623/hysj.48.6.857.51421.

UCL-Geomatics 2017. Land Cover CCI Product User Guide. Technical report, UCL-Geomatics 2017, 2017.

F van Oorschot. *The hydrologically active rootzone in climate models*. PhD thesis, University of Technology Delft, 2020. URL https://repository.tudelft.nl/islandora/object/uuid{%}3A8d4da9f5-fd23-487a-baaf-a255600a5076?collection=education.

Ype Van Der Velde, Nikki Vercauteren, Fernando Jaramillo, Stefan C Dekker, Georgia Destouni, and Steve W Lyon. Exploring hydroclimatic change disparity via the Budyko framework. *Hydrological Processes*, 4118(July 2013):4110–4118, 2014. doi: 10.1002/hyp.9949.

R P D Walsh and D M Lawler. RAINFALL SEASONALITY: DESCRIPTION, SPATIAL PATTERNS AND CHANGE THROUGH TIME. *Weather*, 36(7):201–208, 1981. ISSN 0043-1656. doi: doi:10.1002/j.1477-8696.1981.tb05400.x. URL https://doi.org/10.1002/j.1477-8696.1981.tb05400.x.

L Wang-Erlandsson, W G M Bastiaanssen, H Gao, J Jägermeyr, G B Senay, A I J M van Dijk, J P Guerschman, P W Keys, L J Gordon, and H H G Savenije. Global root zone storage capacity from satellite-based evaporation. *Hydrol. Earth Syst. Sci.*, 20(4):1459–1481, 2016. ISSN 1607-7938. doi: 10.5194/hess-20-1459-2016. URL `https://www.hydrol-earth-syst-sci.net/20/1459/2016/`.

L. Zhang, W. R. Dawes, and G. R. Walker. Response of mean annual evapotranspiration to vegetation changes at catchment scale. *Water Resources Research*, 2001. ISSN 00431397. doi: 10.1029/2000WR900325.